



UNIVERSITEIT•STELLENBOSCH•UNIVERSITY
jou kennisvenoot • your knowledge partner

Irreversible Demagnetization of Permanent Magnets under Short-Circuit Conditions in Permanent Magnet Synchronous Machines

Ian Paul Gerber
21011788

Report submitted in partial fulfilment of the requirements of the module
Project (E) 448 for the degree Baccalaureus in Engineering in the Department of
Electrical and Electronic Engineering at Stellenbosch University.

Supervisor: Prof. R.J. Wang
Supervisor: Dr. S. Gerber

November 2020

Acknowledgements

I would like to thank the following people for their direct or indirect contribution to my Skripsie:

- Doctor Stiaan Gerber and Professor Rong-Jie Wang for their knowledge, guidance, patience and time.
- Stravos Pastellides for his help with material for a case study.
- All lecturers and staff of the Engineering Faculty and specifically the Electrical and Electronic department for preparing us for the world of engineering outside the faculty and this project.
- Francois du Plessis for answering good and bad questions for four years and his and Abraham "Awie" Botes's help with access to Ansys Maxwell.
- Doctor Herman Kamper for the Skripsie-template.
- Professor Thinus Booysen for his report video.
- My family and Jeanri Nel.
- God, my Father, for His grace, mercy and overwhelming love and His Son, Jesus Christ for hope.
- Paul Gerber.



UNIVERSITEIT • STELLENBOSCH • UNIVERSITY
jou kennisvennoot • your knowledge partner

Plagiaatverklaring / *Plagiarism Declaration*

1. Plagiaat is die oorneem en gebruik van die idees, materiaal en ander intellektuele eiendom van ander persone asof dit jou eie werk is.

Plagiarism is the use of ideas, material and other intellectual property of another's work and to present it as my own.

2. Ek erken dat die pleeg van plagiaat 'n strafbare oortreding is aangesien dit 'n vorm van diefstal is.

I agree that plagiarism is a punishable offence because it constitutes theft.

3. Ek verstaan ook dat direkte vertalings plagiaat is.


I also understand that direct translations are plagiarism.

4. Dienooreenkomstig is alle aanhalings en bydraes vanuit enige bron (ingesluit die internet) volledig verwys (erken). Ek erken dat die woordelike aanhaal van teks sonder aanhalingstekens (selfs al word die bron volledig erken) plagiaat is.

Accordingly all quotations and contributions from any source whatsoever (including the internet) have been cited fully. I understand that the reproduction of text without quotation marks (even when the source is cited) is plagiarism.

5. Ek verklaar dat die werk in hierdie skryfstuk vervat, behalwe waar anders aangedui, my eie oorspronklike werk is en dat ek dit nie vantevore in die geheel of gedeeltelik ingehandig het vir bepunting in hierdie module/werkstuk of 'n ander module/werkstuk nie.

I declare that the work contained in this assignment, except where otherwise stated, is my original work and that I have not previously (in its entirety or in part) submitted it for grading in this module/assignment or another module/assignment.

21011788	
Studentenommer / <i>Student number</i>	Handtekening / <i>Signature</i>
I. P. Gerber	01/11/2020
Voorletters en van / <i>Initials and surname</i>	Datum / <i>Date</i>

Abstract

English

Currently, the Finite Element Method is used to analyse Permanent Magnet Synchronous Machines. This method can be time consuming and complex for transient analysis. During a three-phase short-circuit, a Permanent Magnet Synchronous Machine's magnet can become demagnetized. This damaged magnet has a negative influence on the operation of the machine.

The main aim of this project is to investigate the effect of irreversible demagnetization of permanent magnets under three-phase short-circuit conditions in Permanent Magnet Synchronous Machines and the change in the machine's characteristics.

Although investigations has been conducted in this field, it has not been done for Stellenbosch's own Finite Element Method, SEMFEM. There is also little research on the operation of a machine after a short-circuit has occurred.

With the use of numerical methods in Python, the dynamic behaviour of dq-currents could be effectively and thoroughly analysed after a short-circuit. Multiple methods were used to decrease the simulation time.

An effective method was implemented to witness the effect of a three-phase short-circuit on the operation of a Permanent Magnet Synchronous Machine.

Afrikaans

Daar word huidiglik op die Eindige Element Metode staat gemaak om Permanente Magneet Sinchrone Masjiene te analiseer. Hierdie metode kan tydrowend en kompleks word vir kortstondige analises. Gedurende 'n drie-fase kortsluiting kan 'n Permanente Magneet Sinchrone Masjien se magneet beskadig word. Die beskadigde magneet het 'n negatiewe invloed op die werking van die masjien.

Die hoofdoel van die projek is om die effek van onomkeerbare demagnetisering in 'n Permanente Magneet Sinchrone Masjien onder kortsluiting toestande te ondersoek en die

invloed daarvan op die masjien se eienskappe.

Alhoewel daar alreeds studies in hierdie veld gemaak is, is dit nog nie in Stellenbosch se eie Eindige Element Metode program, SEMFEM, geïnkorporeer nie. Daar is ook min ondersoek ingestel in die werking van die Permanente Magneet Sinchrone Masjien na 'n kortsluiting.

Met die gebruik van numeriese metodes in Python, kon die dinamiese dq-strome effektief en deeglik geanaliseer word na 'n kortsluiting. Verskeie metodes is gebruik om die simulاسie so kort moontlik te hou.

'n Effektiewe manier is gevind om die effek van 'n drie-fase kortsluiting op die werking van 'n Permanente Magneet Sinchrone Masjien te vind.

Contents

Abstract	iii
List of Figures	ix
List of Tables	xii
Nomenclature	xiv
1. Introduction	1
1.1. Background	1
1.2. Problem Statement	1
1.3. Project Objectives	2
1.4. Contribution	2
1.5. The Layout of the Report	2
2. Literature Review	3
2.1. Related Work	3
2.1.1. Siemens AG/Siemens Mobility GmbH Research	3
2.1.2. Lappeenranta University of Technology	4
2.1.3. Vienna University of Technology	4
2.2. Permanent Magnets During Three-Phase Short-Circuits	4
3. Detailed Designed	7

3.1. Overview	7
3.2. The Dynamic Short-Circuit	8
3.2.1. Relationship between Flux and Current	8
3.2.2. Dynamic Short Circuit: Change in Flux Linkage	9
3.2.3. Obtaining Current from Flux Linkage	10
3.3. Getting the first Minimum	12
3.3.1. Method 1: Using the second derivative	13
3.3.2. Method 2: Check where gradient's sign change	13
3.3.3. Method 3: Fitting a sine-curve	14
3.4. Analytical Approach to Dynamic Short-Circuit	16
3.4.1. Obtaining the DQ Inductances	16
3.4.2. The Dynamic Short-Circuit	17
3.5. Worst-case Operating Point	18
3.6. Demagnetization due to Three-Phase Short-Circuit in SEMFEM	19
3.7. Application of Demagnetization during Three-Phase Short-Circuit in Opti- mization	19
4. Unit Verification	21
4.1. Own Implementation compared to Scipy	21
4.2. Verifying the Dynamic Behaviour	22
4.3. Testing the Analytical Approach	24
4.4. First Minimum	25
5. Comparison with Transient FEM Simulation and Application During Optimiza- tion	27
5.1. Transient Ansys Maxwell Simulation Comparison	27

5.1.1. First Comparison: Increasing D-axis Current	28
5.1.2. Second Comparison: Decreasing D-axis Current	31
5.2. Application of Three-Phase Short Circuits in Optimization	33
6. Conclusion	37
6.1. Summary	37
6.2. Objectives	37
6.3. Observations	38
6.4. Implications	39
6.5. Future Work	39
Bibliography	40
A. Project Planning Schedule	42
B. Outcomes Compliance	46
B.1. Exit Level Outcome 1: Problem Solving	46
B.2. Exit Level Outcome 2: Application of scientific and engineering knowledge	46
B.3. Exit Level Outcome 3: Engineering design	47
B.4. Exit Level Outcome 4: Investigations, experiments and data analysis . . .	47
B.5. Exit Level Outcome 5: Engineering methods, skills and tools, including information technology	47
B.6. Exit Level Outcome 6: Professional and technical communication	48
B.7. Exit Level Outcome 8: Individual work	48
B.8. Exit Level Outcome 9: Independent learning ability	48
C. Machines Used	49

D. Information for Runge-Kutta 4'th Order Unit Verification	50
E. Reference Guide	51
E.1. Interpolators	51
E.1.1. Obtaining Interpolators	51
E.2. Runge-Kutta	52
E.2.1. Obtaining Dynamic Behaviour for Specified Time Period	52
E.2.2. Obtaining Dynamic Behaviour until First Minimum	53
E.3. Analytical Approach	54
E.3.1. Obtaining Dynamic Behaviour	54
F. Optimizing Results	56
G. Case Study	60

List of Figures

2.1. The BH-curve of a magnetic material [1].	5
2.2.	5
2.3. Equivalent Three-Phase Short-Circuit Space Vector [2].	6
3.1. System Design.	7
3.2. DQ-Magnetic Flux Linkages after a Linear Interpolator was applied.	9
3.3. Inverse Interpolations.	11
3.4. Difference between input and output d-axis currents.	12
3.5. The dynamic behaviour with the initial dq-currents in the four different quadrants	12
3.6. The area required to be identified is in between the two red, dashed lines while using method 1 or when moving from the grey to the yellow block when using method 2.	13
3.7. Finding the minimum d-axis currents with varying flux map accuracies. . .	14
3.8. Results obtained for Germishuizen's machine running at 5000 rpm and 20^2 points used for the flux map.	15
3.9. Inductance Maps obtained.	17
3.10. The minimum d-axis current for the corresponding input dq-currents. . . .	18
3.11. The minimum d-axis current for the corresponding rotational speed.	18
3.12. Procedure used in simulate function during optimizing for demagnetized machine.	20

3.13. Procedure used in simulate function during optimizing for normal and demagnetized machine.	20
4.1. Some of the results obtained.	21
4.2. The machine used by Germishuizen [3] and the recreated version.	22
4.3. The flux linkage behaviour during a dynamic short-circuit at 830 rpm, the red dot depicts the minimum d-axis current.	23
4.4. The dynamic behaviour of the current and flux linkage after a short-circuit as seen from Germishuizen and Adam [3].	23
4.5. The dynamic behaviour of the current and flux linkage after a short-circuit.	24
4.6. The analytical Method compared to the Runge-Kutta method for rpm = 5000 rot/min.	24
4.7. The analytical Method compared to the Runge-Kutta method for rpm = 830 rot/min.	25
4.8. The dynamic behaviour of the current and flux after a short circuit up to various times with the aim to get the first minimum.	26
5.1. The SEMFEM and Ansys Maxwell implementation of the machine in steady-state.	27
5.2. Machine 3, as described in Appendix C.	28
5.3. Short circuits occur at $t = 0.1$ s and 0.3 s while normal steady state conditions exist up until 0.1 s, between 0.2 and 0.3 s as well as from 0.4 s.	28
5.4. The procedure followed in SEMFEM.	29
5.5. DQ-currents as determined in this project.	30
5.6. The dynamic behaviour of the dq-currents after a short circuit, compared to the Ansys Maxwell implementation.	31
5.7. Short circuits occur at $t = 0.1$ s and 0.3 s while normal steady state conditions exist up until 0.1 s, between 0.2 and 0.3 s as well as from 0.4 s.	32

5.8. The dynamic behaviour of the dq-currents after a short circuit, compared to the Ansys Maxwell implementation.	33
5.9. Normal Optimization	34
5.10. Optimization with Demagnetization Constraint	34
5.11. Optimization for Demagnetized Machine	35
5.12. Optimization for Demagnetized Machine and its Normal Operating Point .	35
A.1. Planning 1.a	42
A.2. Planning 1.b	43
A.3. Planning 2.a	44
A.4. Planning 2.b	45
G.1. The machine configuration after optimizing for different operating points w.r.t. demagnetization.	61

List of Tables

3.1. The deviations from the linear interpolator's output in percentage.	9
3.2. The amount of steps required for the smallest error for machine 1 for different flux map densities.	15
3.3. The amount of steps required for the smallest error for machine 2 for different flux map densities.	16
4.1. The comparison between the two machines at 5000 rpm	23
5.1. Torque performance	30
5.2. Torque performance	32
5.3. Some parameters of the optimized machines.	36
C.1. The specifications of the different machines used in this project.	49
F.1. Optimize Spreadsheet Inputs and Outputs Configuration. The only differ- ence would be for optimizing with a demagnetization constraint where a constraint would be added.	57
F.2. The Optimized Outputs.	59
G.1. The torque and efficiency output after multiple short-circuits at the normal operating speed.	60
G.2. The torque and efficiency output after multiple short-circuits at full speed.	60
G.3. The torque and efficiency output after multiple short-circuits at normal speed for the new machine.	61

G.4. The torque and efficiency output after multiple short-circuits at full speed for the new machine.	61
---	----

Nomenclature

Variables and functions

B	Magnetic Flux Density.
H	Magnetic Field Strength.
T	Torque.
ω	Angular frequency.
f	Frequency.
μ	Material's magnetic permeability.
ψ	Magnetic Flux linkage.
Ω	Resistance.
V	Voltage.
I	Current.
P	Power.
θ	Angle.
n_s	Synchronous speed.

Acronyms and abbreviations

MMF	Magnetomotive Force
PMSM	Permanent Magnet Synchronous Motor
FEA	Finite Element Analysis
FEM	Finite Element Method
ITSF	Inter Turn Short Fault
SEMFEM	Stellenbosch Electrical Machines Finite Element Method
EV	Electric Vehicle
LEV	Light Electric Vehicle

Chapter 1

Introduction

1.1. Background

Electric vehicles (EV) are increasingly used in both urban and industrial environments. Electric motors are the essential part of the EV power train systems. Different types of electric motor technologies have been developed for this purpose. Amongst others, Permanent Magnet Synchronous Motors (PMSM) are widely used for EV applications because of their unique advantages such as high efficiency and high power density. However, permanent magnets are inherently sensitive to both temperature and operation related demagnetization risks. These important aspects need to be carefully analyzed and considered during the design stage of Permanent Magnet motors. At Stellenbosch University, SEMFEM, Stellenbosch Electrical Machines Finite Element Method, can be used for a Finite Element Analysis (FEA).

1.2. Problem Statement

The main aim of the project is to investigate the effect of irreversible demagnetization of permanent magnets under three-phase short-circuit conditions in Permanent Magnet Synchronous Machines and the change in the machine's characteristics. Traditionally, transient finite element analysis is required to simulate the operating characteristics under such conditions, which are computationally very expensive. In this project, an efficient analytical method will be implemented to perform such calculations within a short period of time.

Different short-circuits were outside the scope of this project, i.e. only three-phase short-circuits were analysed. Phase-to-earth, phase-to-phase-to-earth and phase-to-phase short-circuits were neglected. Only PMSM's were considered.

1.3. Project Objectives

Primary objectives in this project are:

1. Develop an accurate prediction of dq-currents after a three-phase short-circuit occurs without a transient FEA.
2. Determine the effect of the most negative d-axis current on the demagnetization of the permanent magnet in a PMSM.
3. Optimize a PMSM, taking into account the effect of a possible three-phase short-circuit.

1.4. Contribution

During this project, the author developed an accurate prediction of the dynamic behaviour of dq-currents after a three-phase short circuit and the effect it has on the permanent magnet and the machine's characteristics. This was implemented in Stellenbosch University's own FEM, SEMFEM. SEMFEM now has the attribute of an analysis of the demagnetization of a permanent magnet under three-phase short-circuit conditions.

1.5. The Layout of the Report

In chapter 2 a literature review is conducted. This review contains previous research in this field and basic PMSM concepts required to conduct this project. Chapter 3 continues with the specific system design and solutions used to solve the problem. These solutions are individually verified in chapter 4 and then the whole system is compared to a transient FEA in Ansys Maxwell in chapter 5 - which contains the results, followed by the conclusion. Appendix E has a reference guide for the functions built. Appendix G has an applicable case study.

Chapter 2

Literature Review

2.1. Related Work

Limited research has been done on the demagnetization analysis of PMSMs under three-phase short-circuit conditions [2–4]. Almost no work can be found in literature regarding how this affects the PMSM’s steady-state performances after multiple short-circuit dissidences and taking a short-circuit into account when designing a machine.

2.1.1. Siemens AG/Siemens Mobility GmbH Research

An article titled **Integrating FEM and existing traction motor design tools into an everyday engineering environment** [3] by Johannes Germishuizen and Christoph Adam, who both work for Siemens AG/Siemens Mobility GmbH Research in Nuremburg, was published in 2019. This article describes a method used to supplement a FEA with a calculation of the dynamic three-phase short-circuit of a PMSM. This was done by solving differential equations, at the time of a short circuit, numerically from characteristics obtained with a FEA at steady-state. The approach aimed to find the behaviour of the torque during the time elapsed shortly after the short-circuit. Emphasis was also placed on integrating the FEM with this specific analysis and other FEM tool-chains.

This article was an excellent source of information during the project. A very similar approach was used to obtain the minimum d-axis current. The approach did not consider multiple short-circuits and only focused on the PMSM’s behaviour during a short-circuit, not its steady-state behaviour afterwards.

2.1.2. Lappeenranta University of Technology

In a Master's thesis conducted by Dmitry Egorov in 2015 [2] an analytical approach was used to obtain the most negative d-axis current. The objective was to find an analytical method to obtain the distribution of the magnetic flux density of a PMSM during steady-state and a three-phase short-circuit. This was done by describing the dynamic behaviour of a short-circuit mathematically and then obtaining the required information from the equivalent circuit of a PMSM - combining the space vector theory with the magnetic circuit. This approach has limited accuracy over a variety of PMSM configurations. The dynamic behaviour of dq-currents were not accurate compared to the corresponding FEM. The study did not investigate lasting effects on steady-state performance.

2.1.3. Vienna University of Technology

In 2010 Andreas Eilenberger and Manfred Schrödl from Vienna University of Technology released an article [4] in which they developed a method to analyse dynamic short-circuits in PMSM's with interior magnets. They made use of a frequency domain analysis of characteristic equations to obtain a mathematical model for the d-axis current. They made use of normalized values. Although this method is very accurate when implemented, more information is required than is generally outputted by a FEA in a steady-state analysis.

2.2. Permanent Magnets During Three-Phase Short-Circuits

An unmagnetized magnetic material will have zero magnetic flux density and zero magnetic field strength. This means it will be situated at the origin of the BH curve. When this magnetic material is magnetized by a current, its magnetic flux density and magnetic field strength will increase until $+B_s$ in Fig. 2.1. At this point, even when increasing the magnetic field strength, the magnetic flux density will not be able to increase - as all the magnetic domains of the material are aligned, it cannot be more aligned. When switching off the current, the magnetic field strength will decrease to zero. The magnetic flux density will decrease to its remnant flux density, as it is now magnetized. When a demagnetizing force is applied, by reversing the current, the magnetic field strength will decrease, causing the magnetic flux density to also decrease.

PMSM's permanent magnet normally operate in the second quadrant of a BH curve.

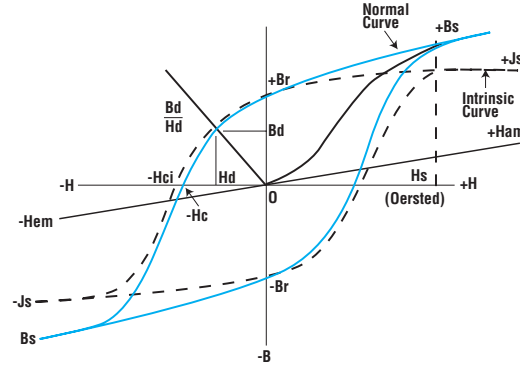
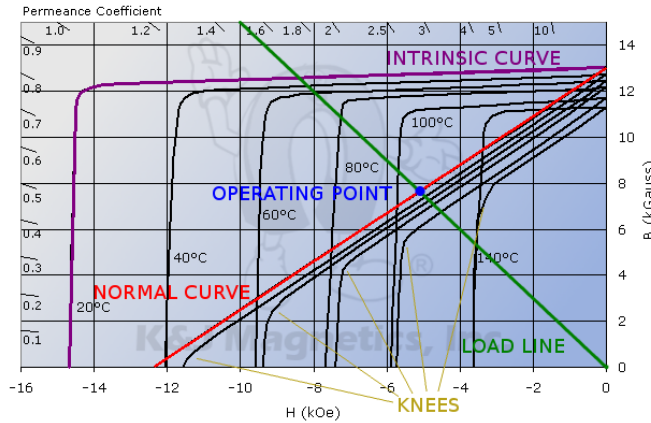
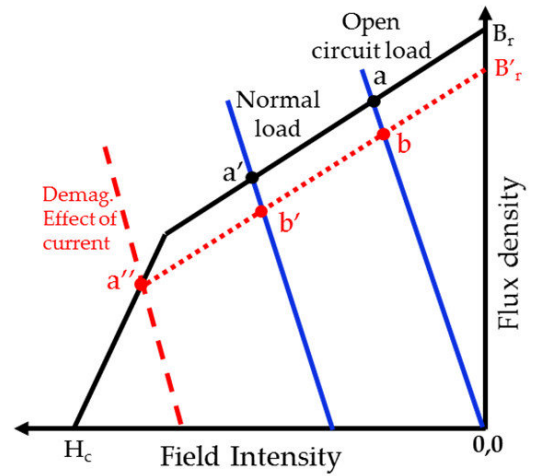


Figure 2.1: The BH-curve of a magnetic material [1].

This is because stator currents causes the magnetic field strength to be negative. It can be seen that the demagnetization curve of a PMSM differs a bit from the normal BH curve. This is because of the air gap in the machine. The intrinsic curve is less linear and does not take the airgap into account nor the spaces between pole pairs. The normal curve is of concern. The knee point is the point where the linear relationship between B and H ends when decreasing the magnetic field strength. The machine operates at the point where the load line/operating slope and the normal curve intersects [5].



(a) Demagnetization Curves [5].



(b) The effect of Irreversible Demagnetization [6].

Figure 2.2

Irreversible Demagnetization can occur due to various reasons: large temperatures while in use, reducing flux, an Inter Turn Short Fault (ITSF), long periods of use, damage to a machine's structure or geometry, an open circuit and a short circuit [6].

Irreversible Demagnetization occurs when the operating point goes beyond the knee point and changes the magnetic characteristics of the machine. This influences all the

capabilities of the machine as the permanent magnet is a fundamental component of the machine. As seen in Fig. 2.2b the operating point moves from a to a' and then past the knee point to a'' as the H-field is weakened. When the H-field increases again, it does not go back to a' and a, but continues through b' and b to the new residual Magnetic Flux Density [6].

According to Haylock, Hoefer and Jack [7] the following are responsible for the **level** of demagnetization: material of the magnet, temperature, the PMSM's geometry, the stator current's magnitude and phase. The MMF produced by the most negative d-axis current has the biggest effect on the demagnetization of the permanent magnet [8] due to flux linkage weakening. If stator resistance is neglected, the space vector model of a PMSM can be seen in Fig. 2.3 [2]. ψ_{p0} is the permanent magnet's flux linkage during steady-state, $\psi_p(t)$ is the permanent magnet's flux linkage after a short-circuit occurs. $L_d i_{d0}$ and $L_q i_{q0}$ is the flux linkages developed in the windings during steady state, while ψ_0 is the flux linkage of the stator during steady-state. When $\psi_p(t)$ and ψ_0 is in directly opposite directions, the maximum demagnetization normally occurs, depending on the permanent magnet's shape, as this is the point the d-axis current is normally also most negative.

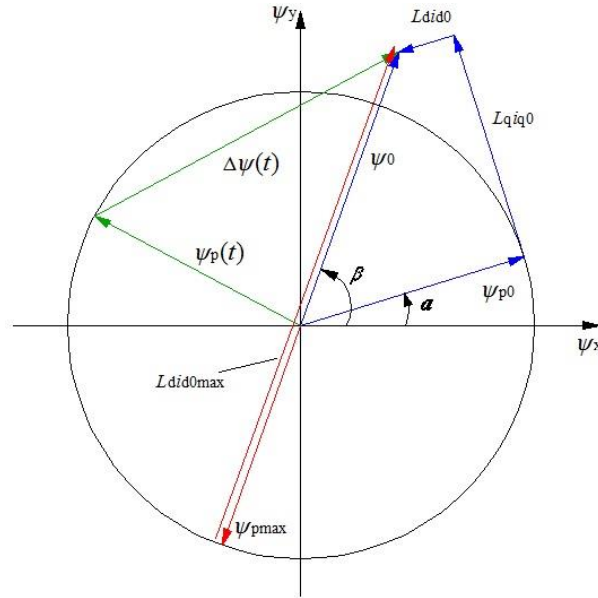


Figure 2.3: Equivalent Three-Phase Short-Circuit Space Vector [2].

Chapter 3

Detailed Designed

3.1. Overview

The methodology used is a mixture of a method proposed by Adam and Germishuizen [3] and Dr. Gerber [9]. Fig. 3.1 summarizes the concept:

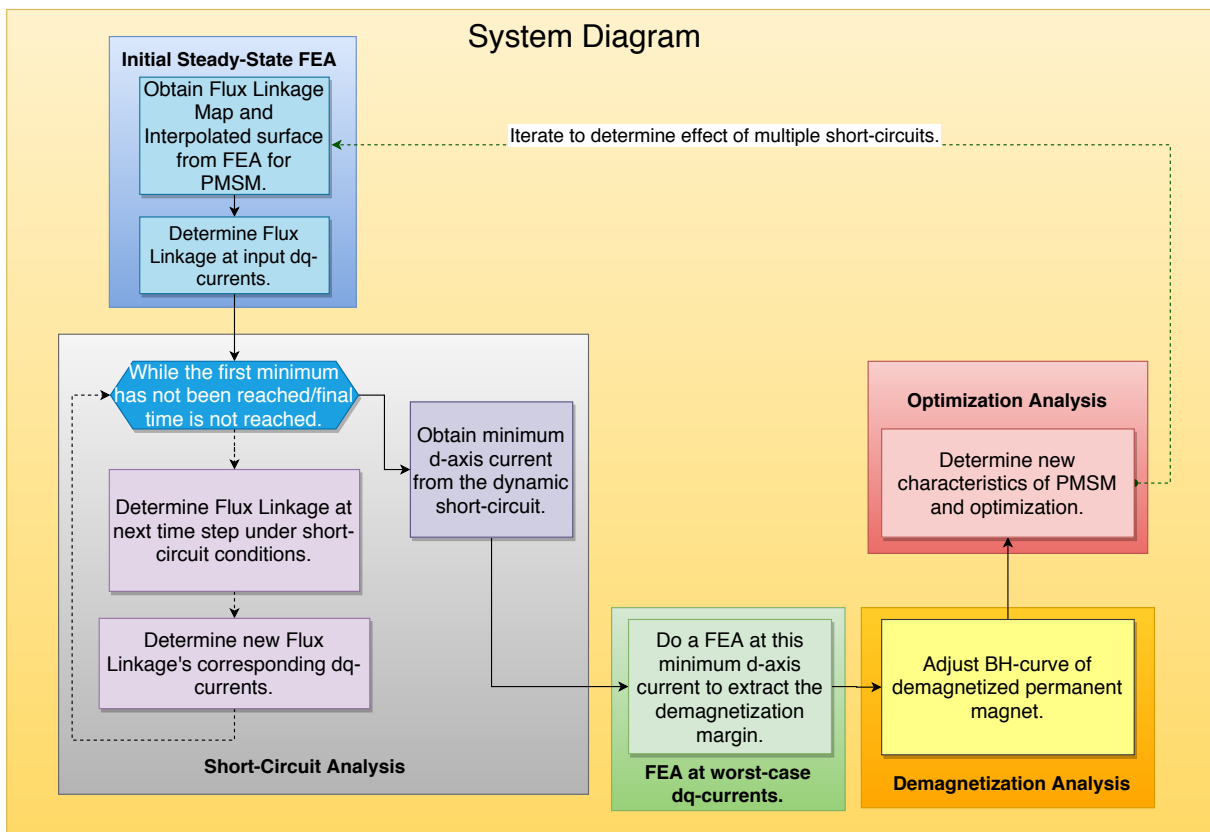


Figure 3.1: System Design.

A normal FEA, the demagnetization and optimization is already implemented in SEMFEM. The dq-currents' behaviour need to be determined. All of the methods above were implemented in Python, which can be integrated with SEMFEM. **A reference**

guide is attached in Appendix E.

3.2. The Dynamic Short-Circuit

To determine to what extent the permanent magnet of the PMSM will be demagnetized, it is necessary to obtain the transient behaviour of the d-axis current after a three-phase short-circuit. First, a flux linkage map is drawn for dq-currents as input. Starting at a specific dq-current combination, the corresponding flux linkages can then be obtained. The next time step's flux linkage can then be found, as the flux linkage changes over time after a short-circuit occurs. For this new flux linkage it is necessary to again obtain the corresponding dq-currents. Looping through this approach the dynamic behaviour over time can be obtained.

3.2.1. Relationship between Flux and Current

When the FEM is applied to a machine, the machine can be simulated over a variety of inputs. For a specific PMSM, with its own unique setup, the corresponding flux linkages for the specific input dq-currents can be found. However, this is done at discrete points. A variety of points scattered in a 3D plane is available. It is required to assess the magnetic flux linkage at any point on a continuous axis. A flux linkage map which is dependent on the input dq-currents is required.

Interpolator

An interpolator can be used to connect points in a 3-D plain, creating a smooth surface. Various types of interpolators exist:

- Linear - Connects the adjacent coordinates directly.
- Nearest-Neighbour - The nearest neighbour method finds the input closest to it from the initial discrete points and gives the new input this z-value.
- Cubic - A third degree polynomial is used to interpolate between points.

To determine the best interpolator, machine 2 as described in Appendix C, was used. First, the interpolator was applied to the grid of dq-currents as inputs, with its corresponding dq-flux linkages. The flux linkage map generated by the linear interpolator

is shown in Fig. 3.2. To compare the difference in output, 100 random dq-currents were generated between -300 and 300 Ampere as input to see the average deviation from the linear interpolator for these 100 inputs.

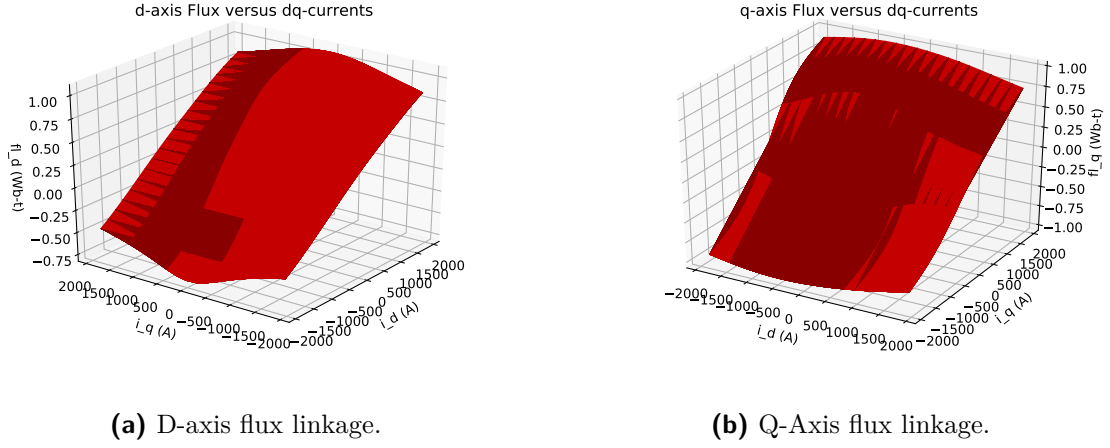


Figure 3.2: DQ-Magnetic Flux Linkages after a Linear Interpolator was applied.

Interpolator	Deviation from linear interpolator (%)	
	D-axis Flux Linkage	Q-axis Flux Linkage
Nearest Neighbour	1.97	1.67
Cubic	0.031	0.028

Table 3.1: The deviations from the linear interpolator's output in percentage.

The deviations between linear, nearest neighbour and cubic interpolators are minute, as shown in Table 3.1. Nearest Neighbour interpolators depend heavily on the grid used - whether it is course or fine. The amount of points used as input currents normally vary between 3 and 20. This means between 9 and 400 points are generated in the 3D plane.

3.2.2. Dynamic Short Circuit: Change in Flux Linkage

The relationship between dq-currents and its flux linkages is now obtained. A PMSM has the following characteristic equations:

$$u_d = R_1 i_d + \frac{d\psi_d}{dt} - \omega_e \psi_q \quad (3.1)$$

$$u_q = R_1 i_q + \frac{d\psi_q}{dt} + \omega_e \psi_d \quad (3.2)$$

When a short-circuit occurs, the dq-voltages will be equal to zero. Equations 3.1 and 3.2 becomes:

$$\frac{d\psi_d}{dt} = -R_1 i_d + \omega_e \psi_q \quad (3.3)$$

$$\frac{d\psi_q}{dt} = -R_1 i_q - \omega_e \psi_d \quad (3.4)$$

Runge-Kutta Fourth-order Method

Germishuizen and Adam [3] used the Runge-Kutta Fourth-order Method to solve for equations 3.3 and 3.4. Other methods could also be used, but the investigation was made with the Runge-Kutta Method. The Runge-Kutta method has an implementation in the Scipy library for Python [10]. It was also implemented from scratch. The applicable Runge-Kutta equations are:

$$y_{n+1} = y_n + \frac{h}{6} \Delta y \quad \begin{cases} \Delta y = \frac{k_1 + 2k_2 + 2k_3 + k_4}{6} \\ k_1 = f'(x_n, y_n) \\ k_2 = f'(x_n + \frac{h}{2}, y_n + \frac{k_1}{2}) \\ k_3 = f'(x_n + \frac{h}{2}, y_n + \frac{k_2}{2}) \\ k_4 = f'(x_n + h, y_n + k_3) \end{cases} \quad (3.5)$$

In our case, $h = dt$ as this is the step size. This was implemented in Python.

3.2.3. Obtaining Current from Flux Linkage

In subsection 3.2.1 a flux linkage map was generated for various dq input currents. In subsection 3.2.2 this map was used to obtain the new flux linkage after each time step during the transient behaviour. It is now important to be able to obtain the corresponding dq-currents for this new flux linkage, as we are interested in the behaviour of the dq-currents and it will be required to obtain flux linkage for the following time step.

Inverse Interpolation

In subsection 3.2.1 a flux linkage map was obtained for the machine, where the dq-magnetic flux linkages are dependent on the dq-currents. To obtain the currents corresponding to the dq-flux linkages, an inverse interpolator could be used, where the currents are a

function of the flux. The resultant 3-D graphs for machine 1 as described in Appendix C is shown in Fig. 3.3.

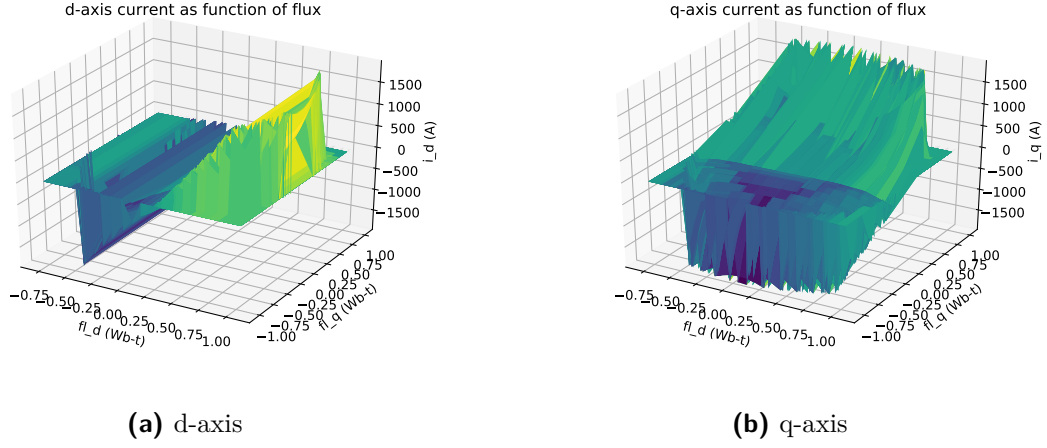


Figure 3.3: Inverse Interpolations.

As can be seen in Fig. 3.3, there exists multiple current values for each combination of dq-flux linkages, i.e. it is not a single-valued function. Due to this reason inverse interpolation cannot be used to find the corresponding currents.

Numerical Methods

A set of non-linear equations describes the flux linkage, this is the functions obtained during interpolation:

$$\psi_d = f(i_d, i_q)$$

$$\psi_q = f(i_d, i_q)$$

Because the flux linkage is only dependent on two variables, Powell's Conjugate Direction or Levenberg-Marquardt algorithms can be applied. If more dimensions were present, Newton's inexact methods would have to be used [10]. These methods obtain the **local** minimum of a function. Powell's Conjugate Direction Method rely on a bi-directional search along vectors. The Levenberg-Marquardt algorithm iteratively changes a parameter vector to obtain the minimum - the initial guess is particularly important.

To test the functionality of the root finding function, a simple test was performed on machine 1. The author looped through all the possible combination of dq-currents. For each combination, its corresponding dq-flux linkages were obtained with the interpolator.

This corresponding flux linkage was then passed to the root function. The difference between the root function's output and the input dq-current combination was obtained - the goal is zero. As seen in Fig. 3.4 only minor errors exist.

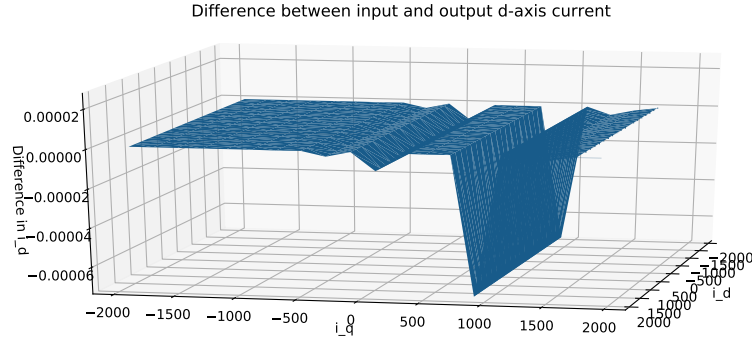


Figure 3.4: Difference between input and output d-axis currents.

3.3. Getting the first Minimum

When analysing the effect of the dynamic behaviour of the machine under a three-phase short-circuit on the demagnetization of the permanent magnet, the most negative d-axis current is of interest, as this is the point at which the most demagnetization of the permanent magnets occur. From Fig. 3.5 the dynamic behaviour at different initial dq-currents operating points can be seen. It is important to note that this behaviour will depend on the machine's geometry and inputs. The "kink" the curve has in Fig. 3.7a is due to coarse flux linkage maps. The flux linkage maps obtained are not dense enough. This whole section made use of machine 1 as described in Appendix C.

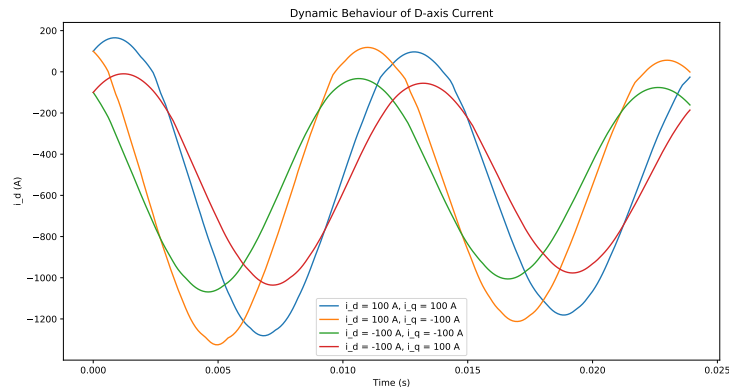


Figure 3.5: The dynamic behaviour with the initial dq-currents in the four different quadrants

3.3.1. Method 1: Using the second derivative

When iterating through the Runge-Kutta method, the iteration needs to end when the d-axis current reaches a minimum, to minimize simulation time. One way of doing this, is to stop as soon as the gradient begins to increase and is positive, i.e. directly after a minimum is found. This area is in between the two red, dashed lines in Fig. 3.6. To ensure the algorithm is robust enough, various gradients between the last three points is checked, not only the last two points. If the algorithm finds that it is decreasing again shortly after the first "minimum," this minimum is rejected, to ensure the algorithm is robust.

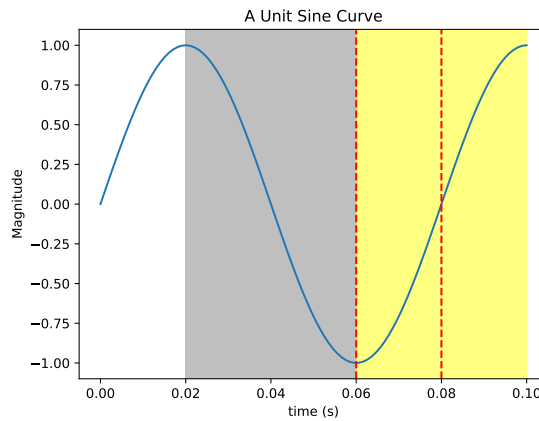
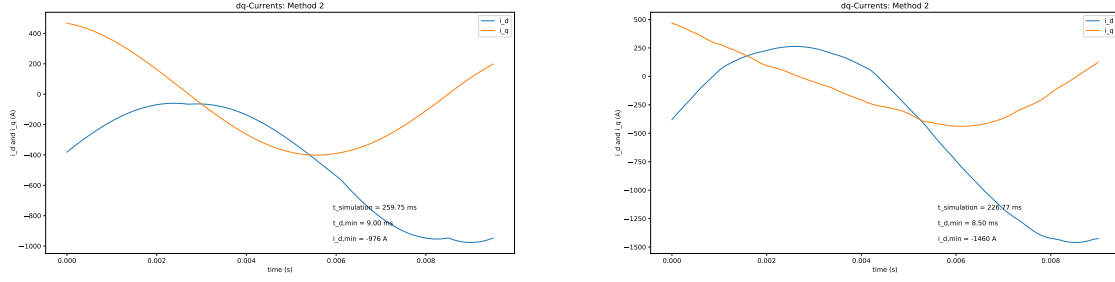


Figure 3.6: The area required to be identified is in between the two red, dashed lines while using method 1 or when moving from the grey to the yellow block when using method 2.

3.3.2. Method 2: Check where gradient's sign change

The sign of the gradient will change at each turning point. The turning point where the gradient changes from a negative (the grey zone in Fig. 3.6) to positive sign (the yellow zone in Fig. 3.6) will indicate a minimum. The algorithm still has to run a certain amount of time steps after this criteria is met to ensure that the curve reaches its real minimum.



(a) The first minimum with a course flux map. (b) The first minimum with a fine flux map.

Figure 3.7: Finding the minimum d-axis currents with varying flux map accuracies.

In Fig. 3.7a the consequences of the amount of points used to create the flux map can be seen. The course flux map in Fig. 3.7a is much less accurate. It does not dip to the real minimum, nor does it reach the correct first peak. This is because the flux map does not contain enough points when generated. However, the first minimum can be found, using this algorithm.

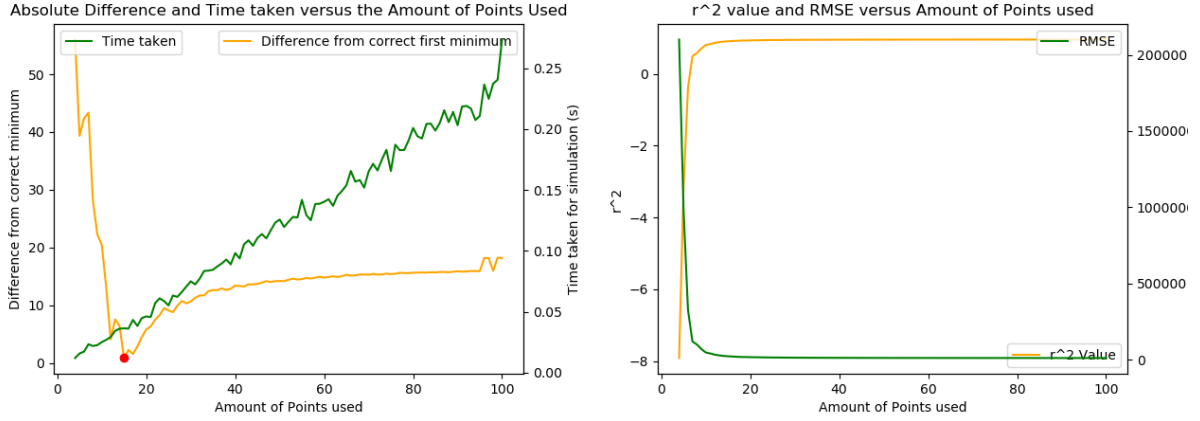
3.3.3. Method 3: Fitting a sine-curve

The third way has the potential to be the quickest method, although it is more complex and difficult to implement a robust algorithm.

$$i_d = e^{\frac{-t}{\tau}} K \sin(2\pi ft + \theta) + d \text{ A} \quad (3.6)$$

Equation 3.6 depicts the general equation describing the waveform we can expect. The dynamic behaviour will decay exponentially. It will oscillate sinusoidally and have some offset.

Equation 3.6 has 4 unknown variables. When implementing the Runge-Kutta method, the time step and end time can be set to ensure integration is only over four steps. From this four points, the required variables can be extracted, by using a least squares estimation. More than four points can be used, but this will have an effect on the time.



(a) The time taken and absolute error when using different amounts of points over which to integrate. (b) The r^2 value and RMSE when using different amounts of points over which to integrate.

Figure 3.8: Results obtained for Germishuizen's machine running at 5000 rpm and 20^2 points used for the flux map.

Our aim is to get the correct first minimum, not to fit the curve perfectly. As seen in Fig. 3.8a, the time increases linearly with the amount of points over which we need to integrate. The closest to the correct minimum is when 15 points is used in this case. As seen in Fig. 3.8b the curve fits very well after approximately 15 points, where the R^2 value almost reaches 1, which means it corresponds well with the real curve, and the RMSE tends to zero for unnormalized data. This, however, does not mean the first minimum is found accurately.

What makes this approach difficult to implement generically, is the amount of points required to be accurate. As seen in Tables 3.2 and 3.3 this is also dependent on the type of machine with no sufficient method to determine a relationship between the amount of points used on the flux linkage map, the geometry and the amount of points required over which to simulate.

Machine 1				
NFM	5	10	15	20
Steps	5	8	14	15

Table 3.2: The amount of steps required for the smallest error for machine 1 for different flux map densities.

Machine 2				
NFM	5	10	15	20
Steps	4	4	4	4

Table 3.3: The amount of steps required for the smallest error for machine 2 for different flux map densities.

3.4. Analytical Approach to Dynamic Short-Circuit

An entirely different method can be used to obtain the transient d-axis current after a short-circuit. The following equations characterize the PMSM w.r.t. inductance instead of flux linkage:

$$u_d = L_d i_d + R i_d - \omega L_q i_q + \omega \psi_{pm} \quad (3.7)$$

$$u_q = L_q i_q + R i_q - \omega L_d i_d \quad (3.8)$$

As seen in equations 3.7 and 3.8, there is numerous information unavailable. The dq-inductances at steady-state and the permanent flux linkage of the magnet is required. This section made use of machine 1 in appendix C.

3.4.1. Obtaining the DQ Inductances

In an article by Johannes Germishuizen and Ronald Tanner [11], a method is proposed to obtain inductances from a steady-state FEA. From a flux linkage map the following equation can be obtained:

$$\psi_d = f(i_d, i_q) \quad (3.9)$$

From equation 3.9 the following can be obtain:

$$\psi_d^d = f(i_d) \mid_{i_q=\text{fixed value}} \quad (3.10)$$

$$\psi_d^q = f(i_q) \mid_{i_d=\text{fixed value}} \quad (3.11)$$

$$\psi_d^0 = \psi_{pm} = f(i_d, i_q) \mid_{i_d=i_q=0} \quad (3.12)$$

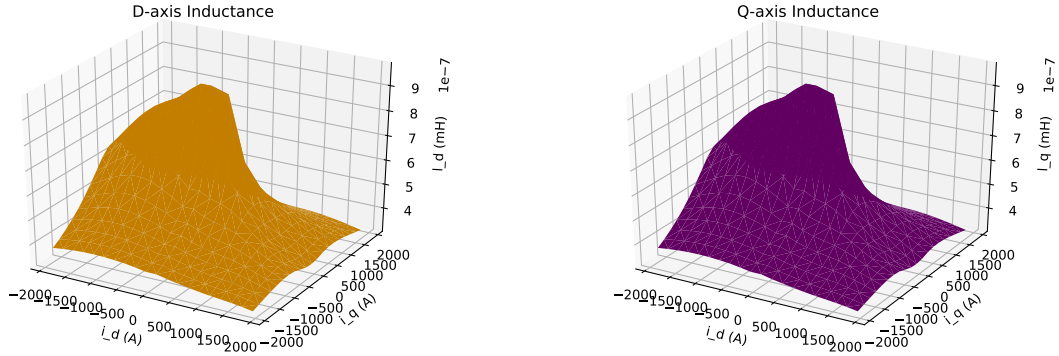
$$\psi_d^q = f(i_q) \mid_{i_d=0} = k_c \psi_{pm} \text{ where } k_c \leq 1 \quad (3.13)$$

We also know:

$$\psi_d = L_d i_d - k_c \psi_{pm} \quad (3.14)$$

$$\psi_q = L_q i_q \quad (3.15)$$

The flux linkage maps are available, $k_c \psi_{pm}$ can be obtained from equation 3.13. All information required to obtain the d-axis inductance, L_d with equation 3.14 is then available. The information to obtain the q-axis inductance, L_q , with equation 3.15 is also available now.



(a) D-axis Inductance.

(b) Q-axis Inductance

Figure 3.9: Inductance Maps obtained.

3.4.2. The Dynamic Short-Circuit

According to an analytical approach [2] the dynamic d-axis current can be described as:

$$i_d = e^{\frac{-t}{\tau}} K_d \sin(\omega_e t + \alpha - \beta) + i_{d,ss} \quad (3.16)$$

Where:

$$K_d = \frac{\sqrt{\psi_d^2 + \psi_q^2}}{L_d} \quad (3.17)$$

$$\tau = \frac{2L_d L_q}{R(L_d + L_q)} \quad (3.18)$$

$$i_{d,ss} = \frac{\omega_e^2 \psi_{pm} L_q}{R^2 + \omega_e^2 L_d L_q} \quad (3.19)$$

β is the angle of the stator's flux linkage, which can be obtained with the dq-flux linkages. α is the permanent magnet's flux linkage angle. The dynamic behaviour of the

d-axis current can be obtained.

3.5. Worst-case Operating Point

The worst case operating point occurs when the permanent magnet's flux linkage has the same magnitude as the stator's flux linkage but in an opposite direction. When the dq-currents have the same magnitude, but the d-axis current is negative and the q-axis current is positive, the most negative d-axis current during a short-circuit will occur. Fig. 3.10 shows the most negative d-axis current for a variety of dq-currents as input.

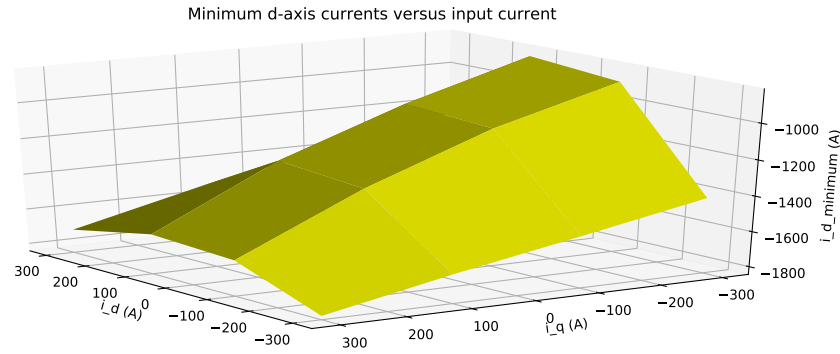


Figure 3.10: The minimum d-axis current for the corresponding input dq-currents.

As can be seen in figure 3.11, the minimum d-axis current decreases with an increase in rotational speed, thus a increase in speed will lead to more demagnetization.

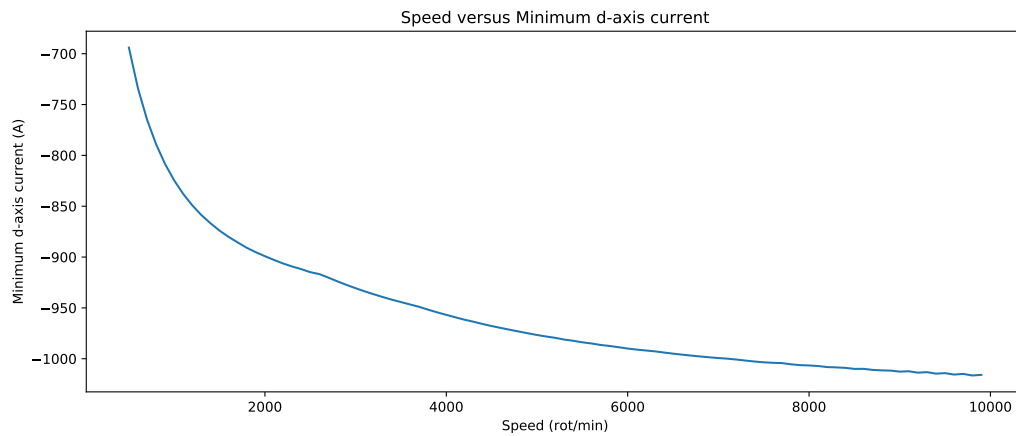


Figure 3.11: The minimum d-axis current for the corresponding rotational speed.

The worst-case operating point is thus at a high speed and dq-currents with equal

magnitude, but different signs.

3.6. Demagnetization due to Three-Phase Short-Circuit in SEMFEM

SEMFEM is able to determine demagnetization that occurs during a simulation and adjust the remnant flux density accordingly. This means that the demagnetization that occurred during a three-phase short-circuit due to the dq-currents can be taken into account by simulating these worst case dq-current combinations whilst applying demagnetization. The author has implemented the calculation of the dq-currents which can now be used to determine the effect the three-phase short-circuit has on the PMSM. The mesh is given a minimum magnetic flux density vector, in this way the permanent magnet is affected in only the regions where demagnetization occurred, not the entire magnet. The minimum magnetic flux density vector is obtained by calculating the operating point on the BH curve of the permanent magnet and adjusting the BH curve if the magnetic flux density is below the knee-point.

3.7. Application of Demagnetization during Three-Phase Short-Circuit in Optimization

SEMFEM has the capability of optimizing a machine, using sequential quadratic programming. This optimization class makes use of the simulation class to simulate a point iteratively. This is usually done for the normal operating speed and the maximum operating speed of the PMSM. Instead of optimizing for these normal operational points, if it is well-known that the machine has a great chance of being short-circuited, optimizing for the demagnetized point as well will be more effective. This can be done by determining the dq-currents after a three-phase short-circuit occurs and the demagnetizing effect it has on the machine, as implemented in this project. It must be noted that the following methodologies are only scratching the surface when integrating this functionality into optimization. A few different methods to optimize are described.

1. **Normal Optimization** - The first methodology used when optimizing is simply to optimize the machine for one or more operating points without demagnetization applied.

2. **Optimizing with Constraints** - Another way to optimize the machine whilst keeping demagnetization in mind would be to optimize a operating point or points with a constraint on the demagnetization allowed. These constraints would optimize the machine to not demagnetize at its normal operating point, it does not take a three-phase short-circuit into account.
3. **Optimizing for a Demagnetized Operating Point** - This methodology is shown in Fig. 3.12. By first simulating a three-phase short-circuit while demagnetization is applied, the machine is demagnetized by this short-circuit. When this demagnetized machine is optimized at its normal operating point, an optimal machine is developed for use after a short-circuit.

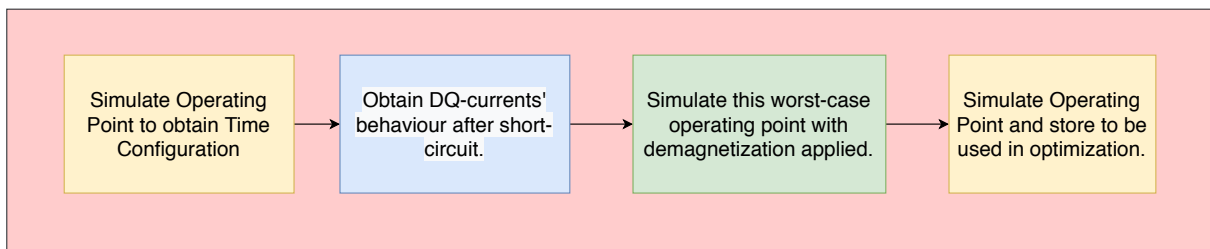


Figure 3.12: Procedure used in simulate function during optimizing for demagnetized machine.

4. **Optimizing for a Demagnetized Operating Point and its Normal Operating Point** - The previous methodology only optimizes a machine after it has been short-circuited. Ideally, the machine also needs to be optimally designed for **normal** operation, i.e. before a short-circuit occurs. We thus simulate for the machine at its normal operating point without demagnetization and after it has been short-circuited. In this way we can also obtain the new optimum operating point after it has been short-circuited. This procedure is shown in Fig. 3.13.

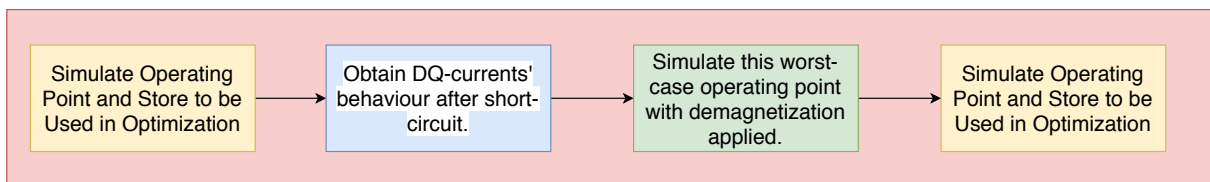


Figure 3.13: Procedure used in simulate function during optimizing for normal and demagnetized machine.

Chapter 4

Unit Verification

4.1. Own Implementation compared to Scipy

The author implemented his own version of the Runge-Kutta method based on previous Python implementations [12]. The different methods were developed and tested on a Kollmorgen 6-pole PM synchronous motor [13], which is not listed in appendix C, where:

$$u_d = R_s i_d + L_d \frac{di_d}{dt} - \omega_e L_q i_q \quad (4.1)$$

$$u_q = R_s i_q + L_q \frac{di_q}{dt} + \omega_e L_d i_d + \omega_e \psi_m \quad (4.2)$$

In the article [13], typical values for a Kollmorgen 6-pole PM synchronous motor driven into saturation is given, as described in Appendix D.

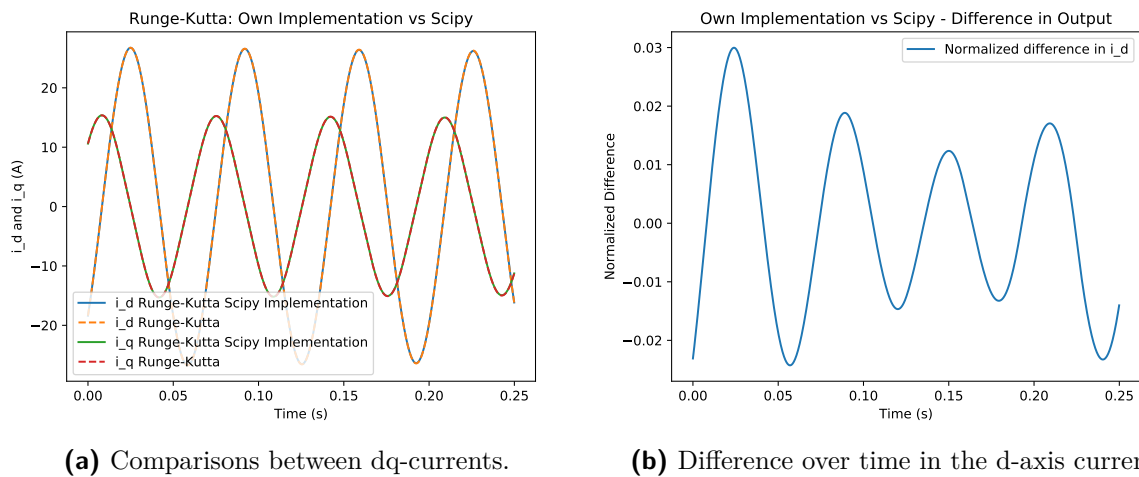


Figure 4.1: Some of the results obtained.

We use this system to test both Runge-Kutta implementations. To simulate a dynamic short circuit, the dq-voltages are set to zero: $u_d = u_q = 0$ and $n = 100$ rpm to make the

oscillations distinguishable. The results for the two different simulations can be seen in Fig. 4.1a.

A slight deviation can be noted between the two methods in Fig. 4.1b. However, this is negligible.

4.2. Verifying the Dynamic Behaviour

To verify that the dynamic behaviour is accurately calculated an attempt was made to compare the output with the output Germishuizen and Adam [3] obtained for a similar method. For this reason the machine they used were recreated in SEMFEM. There was little specific information available to recreate the machine and a lot of assumptions were made - the aim was to have a rough comparison, not a perfect replicate - this is how machine 1's specifications was obtained in Appendix C.

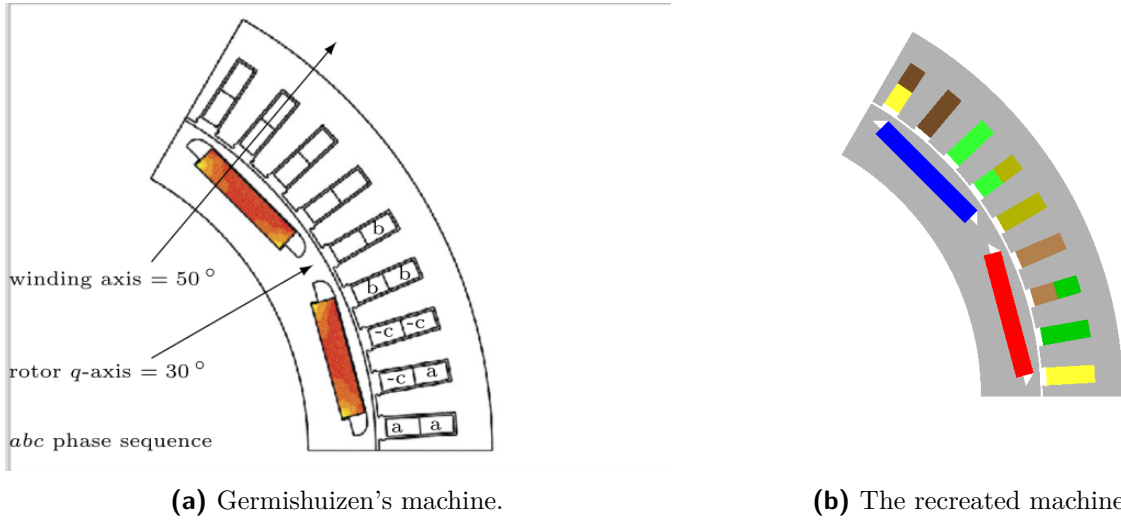


Figure 4.2: The machine used by Germishuizen [3] and the recreated version.

Some information regarding the machine:

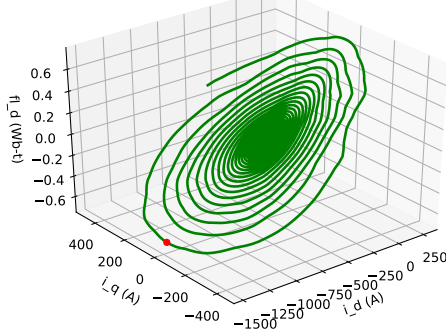
- It is a 260kW, 12 pole PMSM with 54 double-layered slots.
- It has a base speed of 830 rpm.
- $I_{1,max} = 710$ A and their short circuit occurred at $i_d = -381$ A and $i_q = 467$ A
- The winding axis was at 50° and the rotor's q-axis at 30° .
- $B_r = 1.15$ T and the initial winding temperature was 20° C.

- A supply of 530 V and 40 A was specified.
- A fill-factor of 97% was specified.

Table 4.1: The comparison between the two machines at 5000 rpm

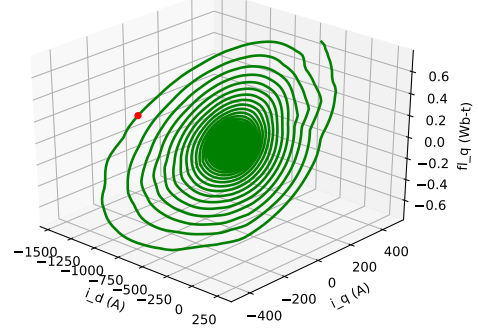
Machine	Comparison	
	Original Machine	Recreated Machine
Torque (Nm)	3200	3028.26
I_1 (A)	420	426.17
U_1 (V)	530	465.48
$I_{d,min}$ (A)	1353	1468.06
ψ_d (Wb-t)	0.15-0.25	0.15
ψ_q (Wb-t)	0.6-0.75	0.7

The dynamic behaviour of the d-axis flux during a short circuit

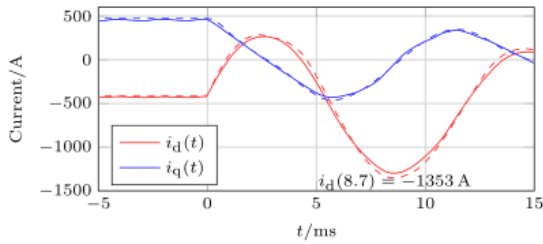


(a) The d-axis flux linkage.

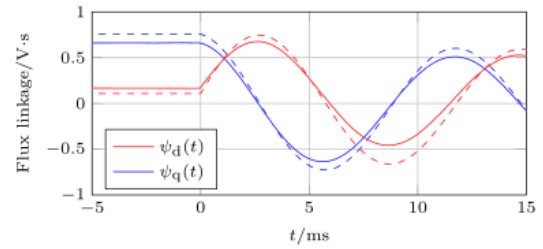
The dynamic behaviour of the q-axis flux during a short circuit



(b) The q-axis flux linkage.

Figure 4.3: The flux linkage behaviour during a dynamic short-circuit at 830 rpm, the red dot depicts the minimum d-axis current.

(a) The currents.



(b) The flux linkages.

Figure 4.4: The dynamic behaviour of the current and flux linkage after a short-circuit as seen from Germishuizen and Adam [3].

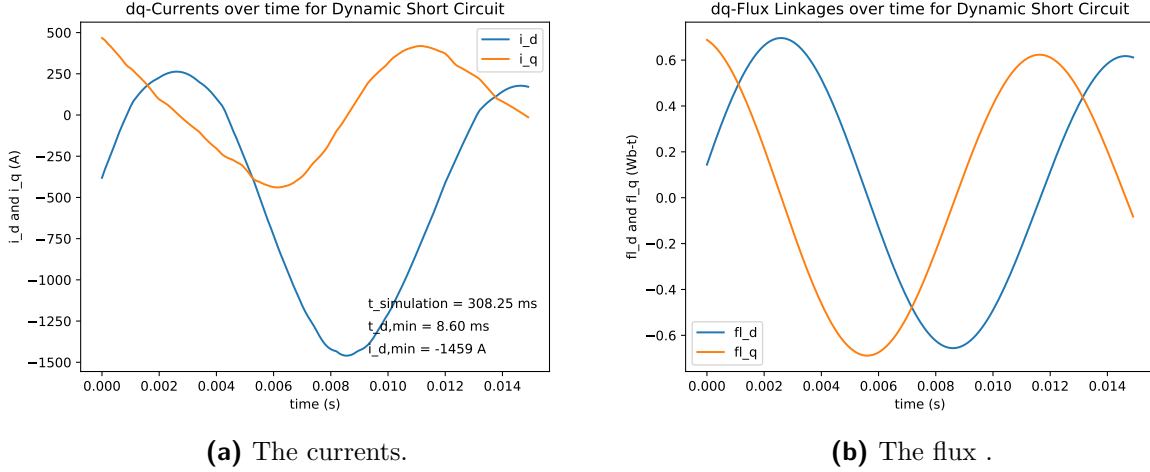


Figure 4.5: The dynamic behaviour of the current and flux linkage after a short-circuit.

4.3. Testing the Analytical Approach

In section 3.4 an alternative approach was used to obtain the d-axis current after a three-phase short-circuit occurs. As expected, the curve has a similar form, with a coefficient of determination of 0.97, but a RMSE of 99 (unnormalized) for a speed of 830 rpm. The approach is able to give a good indication of reality. It was performed on machine 1 in Appendix C.

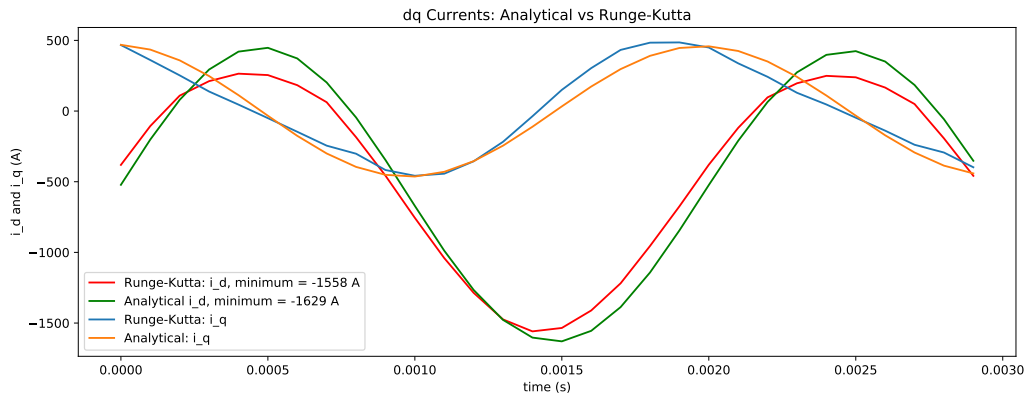


Figure 4.6: The analytical Method compared to the Runge-Kutta method for rpm = 5000 rot/min.

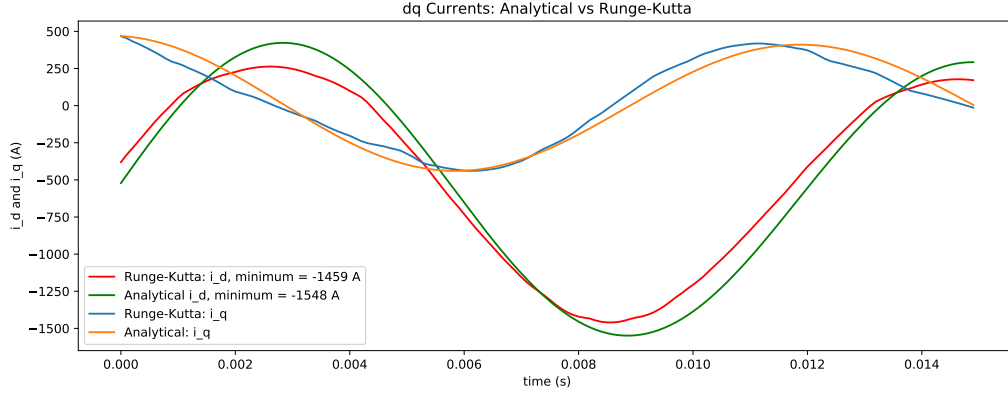
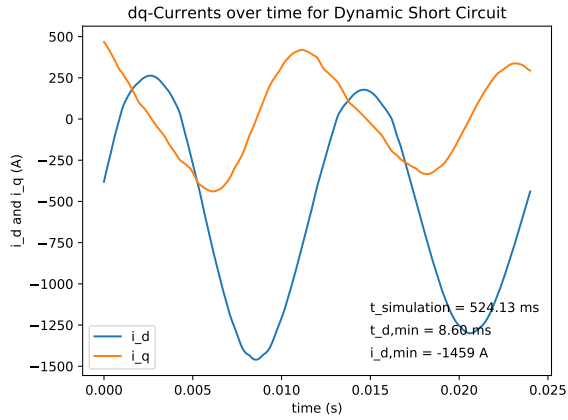


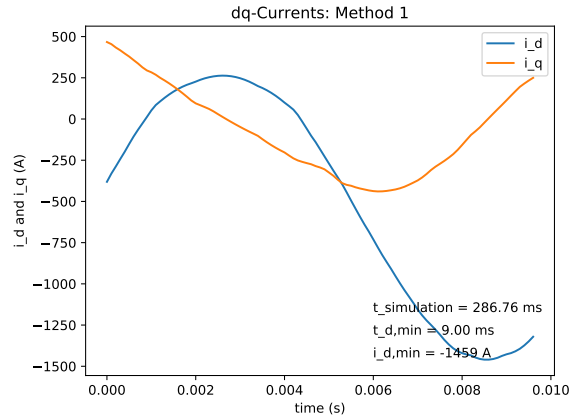
Figure 4.7: The analytical Method compared to the Runge-Kutta method for $\text{rpm} = 830$ rot/min .

4.4. First Minimum

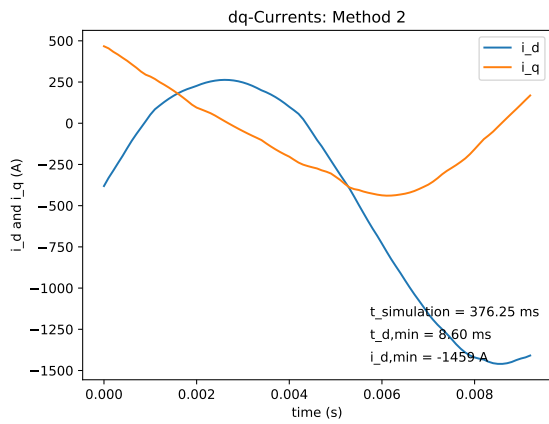
The first minimum for machine 1 was obtained in different ways, as described in section 3.8. As seen in Fig. 4.8, fitting a sine curve to the data is the quickest method to find the minimum, but does not accurately obtain the most minimum point. Method 1 and 2, as described in subsections 3.3.1 and 3.3.2 has similar simulation times and obtains the same value. Simply simulating over a fixed time period takes the longest time and relies on the assumption that the radial frequency remains the same after a short-circuit (which is an accurate assumption as the differential equations confirms this).



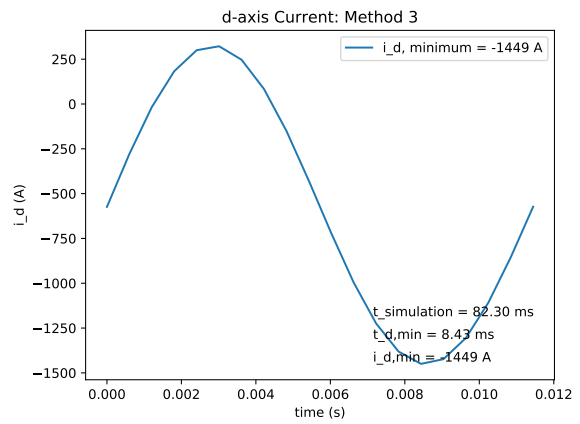
(a) Simulating for two times the period.



(b) Method 1



(c) Method 2



(d) Method 3

Figure 4.8: The dynamic behaviour of the current and flux after a short circuit up to various times with the aim to get the first minimum.

Chapter 5

Comparison with Transient FEM Simulation and Application During Optimization

5.1. Transient Ansys Maxwell Simulation Comparison

To verify the results obtained during this project, machine 3, as described in Appendix C, was built in SEMFEM and Ansys Maxwell. The aim is to determine whether the dq-currents after a three-phase short-circuit correspond and the influence it has on demagnetization. Fig. 5.1 shows steady-state results for both versions to verify that the machines are the same and that similar results should be expected.

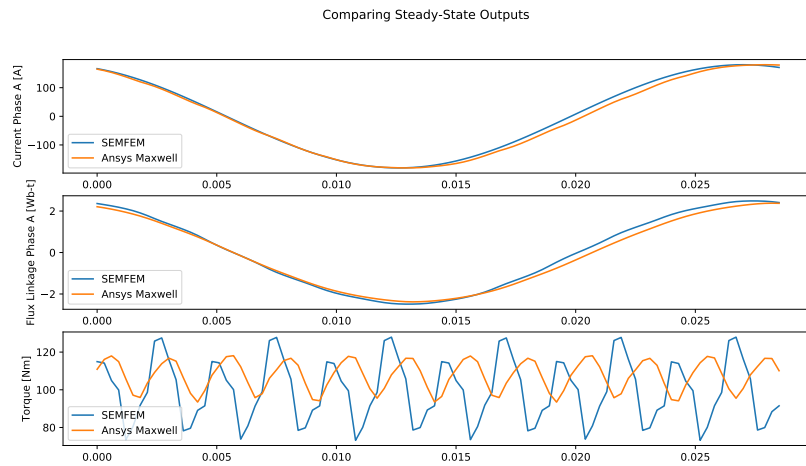


Figure 5.1: The SEMFEM and Ansys Maxwell implementation of the machine in steady-state.

5.1.1. First Comparison: Increasing D-axis Current

Transient Ansys Maxwell Implementation

To ensure Ansys Maxwell results are as applicable as possible, demagnetized operating points were enabled. An external circuit was implemented to induce a short circuit at specified times. A non-linear BH curve was used for Neodymium Iron Boron, the N50 magnet grade at 120°C. An AC control with a Δ -connected source and Y-connected windings was specified in RMxpert, however, when creating a Maxwell 2D design, an external circuit was imported with the Y-Y configuration.

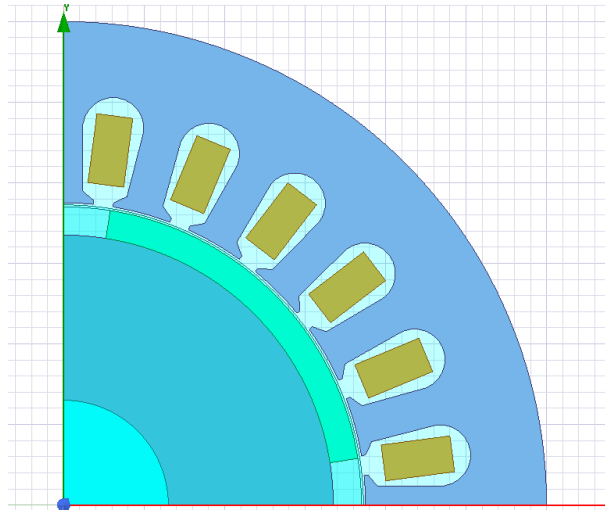
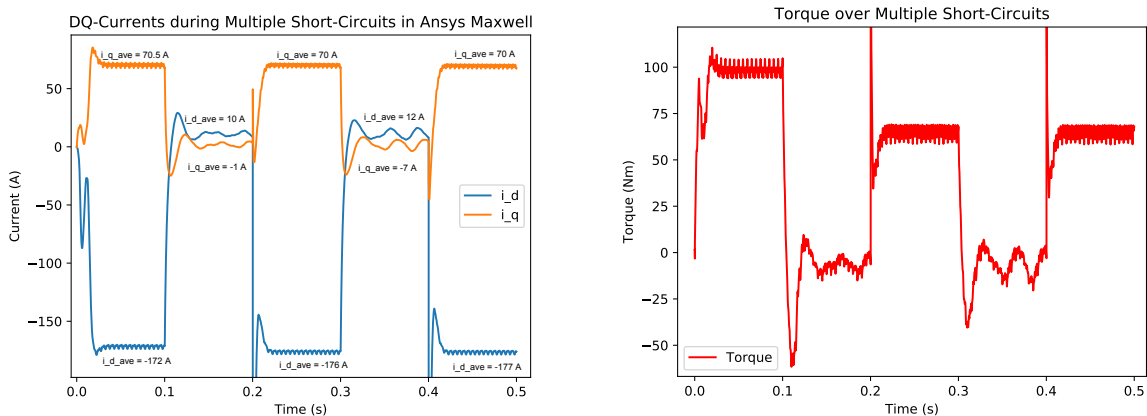


Figure 5.2: Machine 3, as described in Appendix C.



(a) The dq currents over time.

(b) The dynamic behaviour of the torque over the same short-circuit conditions, as described in Fig. 5.7a.

Figure 5.3: Short circuits occur at $t = 0.1$ s and 0.3 s while normal steady state conditions exist up until 0.1 s, between 0.2 and 0.3 s as well as from 0.4 s.

In Fig. 5.7a the dq-currents are shown over a full Ansys Maxwell implementation. A speed of 1000 rpm were used. To witness the effect of multiple short-circuits, it was required to short-circuit the machine multiple times and then reintroduce steady-state operating points. Short circuits occur at $t = 0.1$ s and 0.3 s while normal steady state conditions exist up until 0.1 s, between 0.2 and 0.3 s as well as from 0.4 s. When reconnecting the machine back to the voltage sources a spike in voltage and torque occurs, together with a sharp decrease in d-axis current. In Fig. 5.7b the corresponding torque graph is shown. The average torque at steady-state decreases after each short-circuit.

SEMFEM Implementation

In subsection 5.1.1 the Ansys Maxwell simulation ran over 0.5 s. In SEMFEM the methodology differs. First the initial operating point is simulated. The dq-currents generated during a short-circuit are then calculated for this operating point. These dq-currents are then used as input to simulate the machine again. This sequence is repeated. The average torque at steady state is compared to that of the Ansys Maxwell implementation. The procedure is described in Fig. 5.4. In SEMFEM the corresponding remnant flux density, knee-point and magnetic permeability were used. In Fig. 5.5 we can see the behaviour of the dq-currents. The d-axis current does not decrease to a minimum, but rather increases - this is dependent on the machine's geometry and inputs.

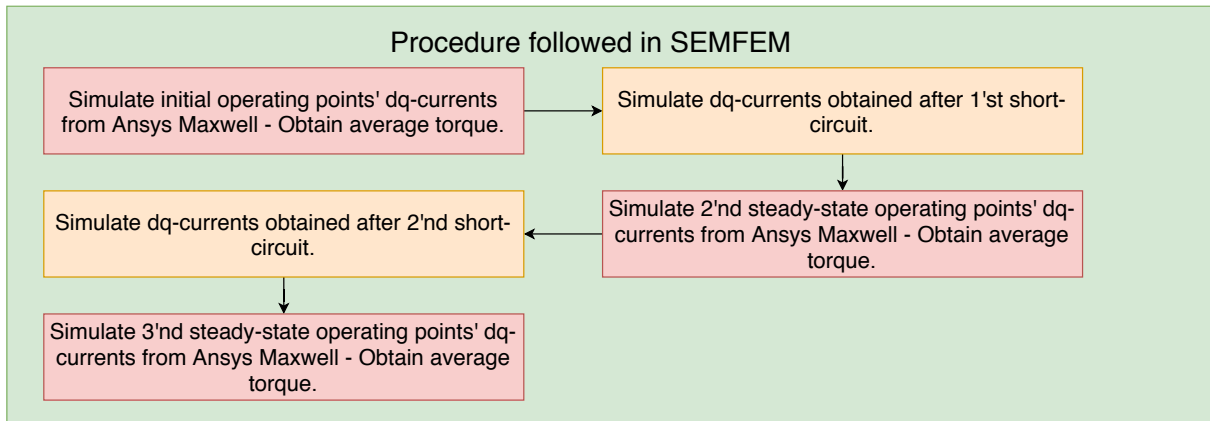


Figure 5.4: The procedure followed in SEMFEM.

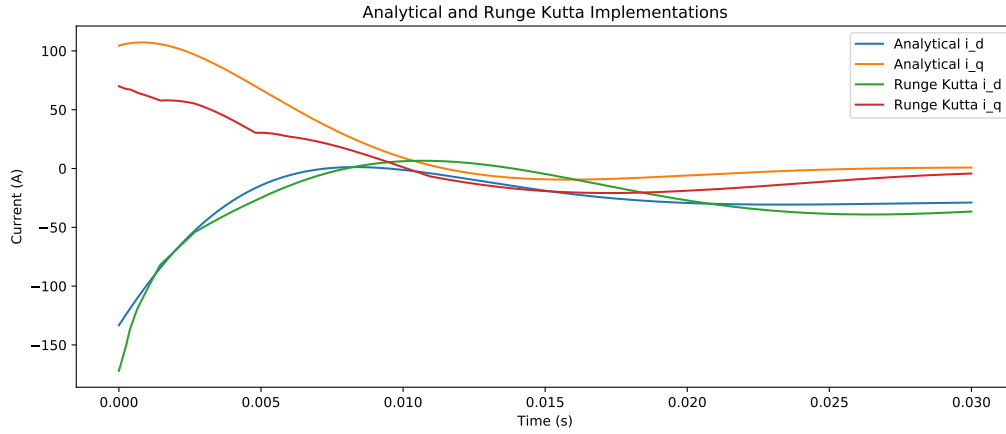


Figure 5.5: DQ-currents as determined in this project.

Comparison

In Table 5.1 the average torque for the Ansys Maxwell and SEMFEM implementations are shown. A normalized value is also shown - these values are normalized w.r.t. the first average torque value obtained during steady-state in Ansys Maxwell.

Comparison in Torque				
	Ansys Maxwell (Nm)	Ansys Maxwell normalized	SEMFEM (Nm)	SEMFEM normalized
Steady State	96.44	1	94.80	0.98
After Short Circuit 1	65.21	0.68	53.17	0.55
After Short Circuit 2	64.96	0.67	48.12	0.5

Table 5.1: Torque performance

In Fig. 5.8 the dq-currents after a three-phase short-circuit in Ansys Maxwell and SEMFEM are shown. The currents generally have the same form, but differ in magnitude. This may be due to various reasons: 1) possible differences in the FEM, SEMFEM and Ansys Maxwell, 2) the effect of the external circuit in Ansys Maxwell and its inductances and resistances, 3) assumptions made in this project w.r.t. the dq-current behaviour during a short-circuit, i.a. the use of steady-state points in developing a flux linkage map, etc.

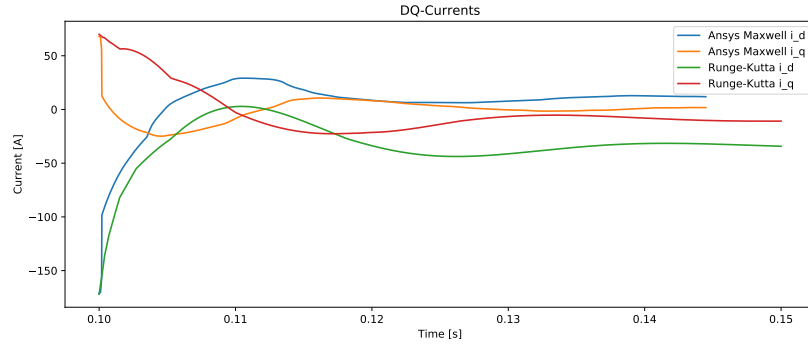


Figure 5.6: The dynamic behaviour of the dq-currents after a short circuit, compared to the Ansys Maxwell implementation.

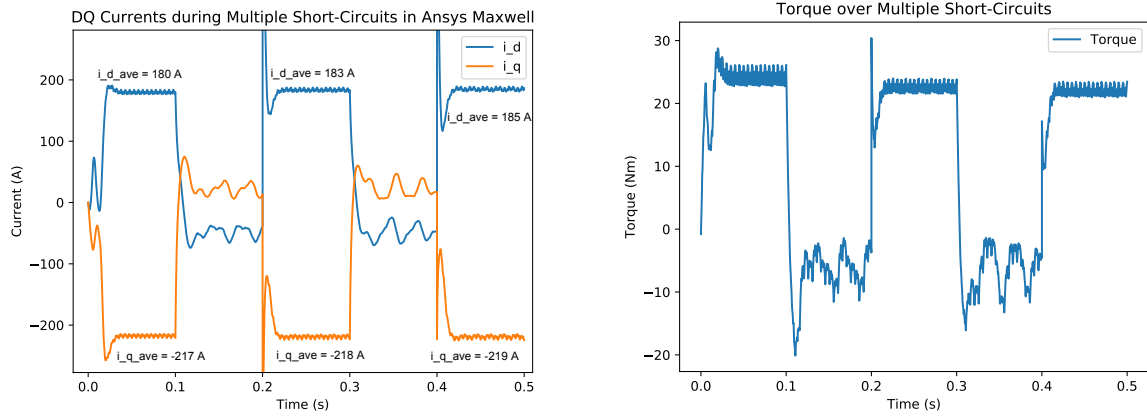
In this comparison we can see that 1) the dq-currents are similar after a short-circuit and 2) that the demagnetization due to its steady-state affects the machine permanently and in a similar value range in SEMFEM and Ansys Maxwell. In this specific situation the d-axis current increased instead of decreased and the effect of this minimum d-axis current could not be witnessed.

5.1.2. Second Comparison: Decreasing D-axis Current

For this verification the machine in section 5.1 is used, but with a decrease in the amount of turns. The same methodology is also followed. The aim is to obtain the effect the minimum d-axis current has on the demagnetization during a three-phase short-circuit. This was not tested in subsection 5.1, as the d-axis current increased.

Transient Ansys Maxwell Implementation

The same methodology is used as in subsection 5.1.1. The only difference is the amount of coil turns. The dq-currents over time, during which two short-circuits occur as well as the output torque is shown in Fig. 5.7.



(a) The dq currents over time.

(b) The dynamic behaviour of the torque over the same short-circuit conditions, as described in Fig. 5.7a.

Figure 5.7: Short circuits occur at $t = 0.1$ s and 0.3 s while normal steady state conditions exist up until 0.1 s, between 0.2 and 0.3 s as well as from 0.4 s.

SEMFEM Implementation

The same methodology is used as in subsection 5.1.1. The only difference is the amount of coil turns and that the minimum d-axis current is simulated, causing demagnetization.

Comparison

In Table 5.2 the resultant torque before and after a three-phase short-circuit can be seen. All normalized values are normalized w.r.t. the steady-state Ansys Maxwell torque output. Fig. 5.8 shows the dq-currents' behaviour after a three-phase short-circuit occurs in Ansys Maxwell and SEMFEM.

Comparison in Torque				
	Ansys Maxwell (Nm)	Ansys Maxwell normalized	SEMFEM (Nm)	SEMFEM normalized
Steady State	24.5	1	24.08	0.98
After Short Circuit 1	22	0.9	22.65	0.92
After Short Circuit 2	22	0.9	20.9	0.85

Table 5.2: Torque performance

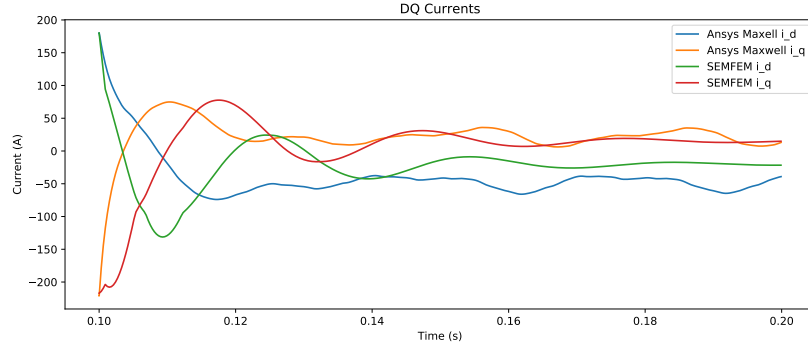


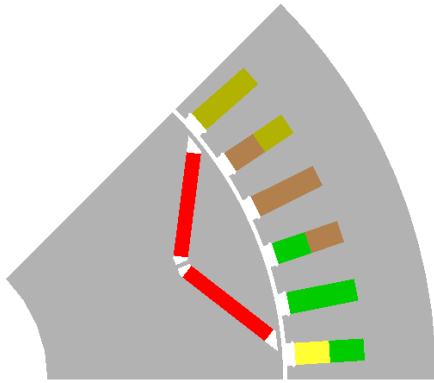
Figure 5.8: The dynamic behaviour of the dq-currents after a short circuit, compared to the Ansys Maxwell implementation.

Summary

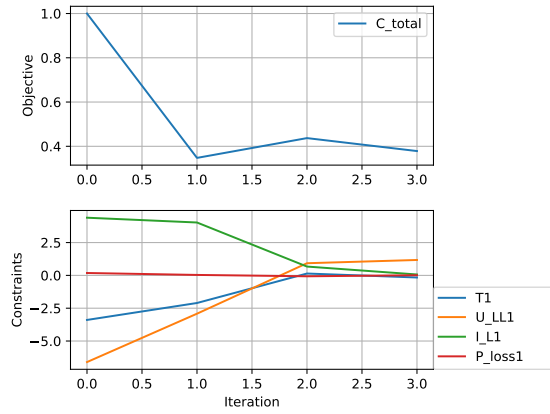
It can be seen that the transient FEA and SEMFEM implementation has similar dq-currents after a three-phase short-circuit, although differences can be witnessed. The influence this three-phase short-circuit has on the performance in steady-state afterwards is very similar. This means we can obtain the effect of the minimum d-axis current on the demagnetization and performance of the machine.

5.2. Application of Three-Phase Short Circuits in Optimization

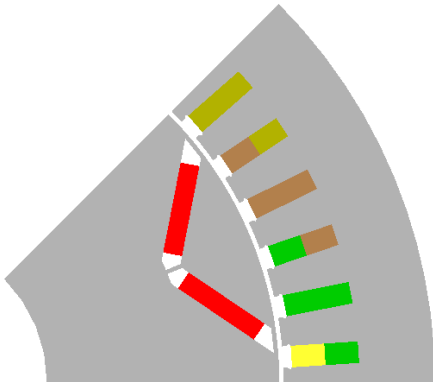
Four different methods to optimize a machine was discussed in section 3.7. The results of simulating with these different procedures for the same initial input variables is shown below. This optimization was performed on machine 4 in Appendix C. In Appendix F the configuration of the optimizing function is shown in Table F.1 and the resultant design outputs is shown in Table F.2.



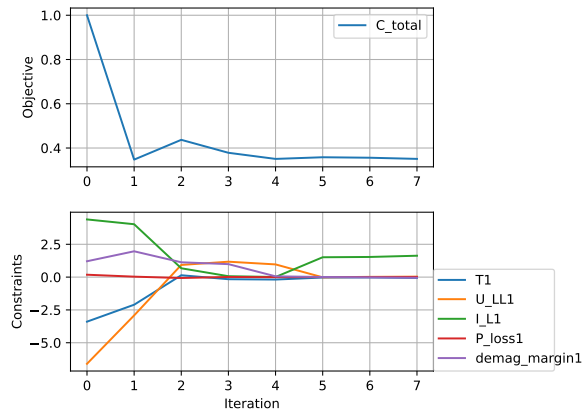
(a) The optimum design.



(b) The change in objective and constraints during optimization.

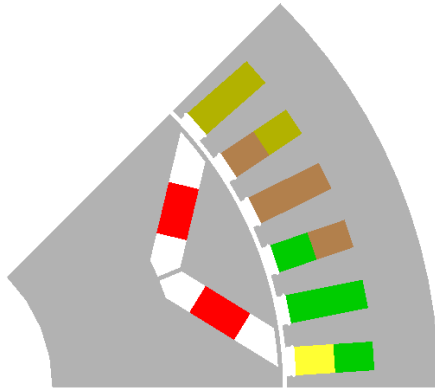
Figure 5.9: Normal Optimization

(a) The optimum design.

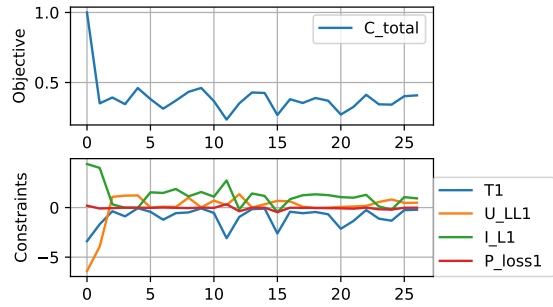
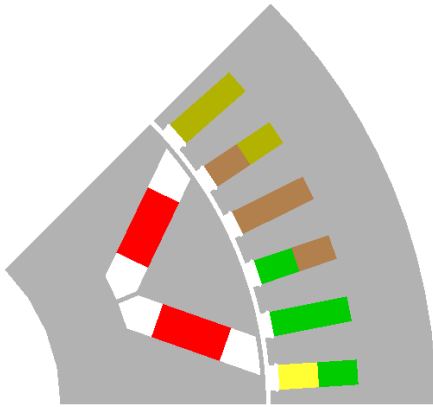


(b) The change in objective and constraints during optimization.

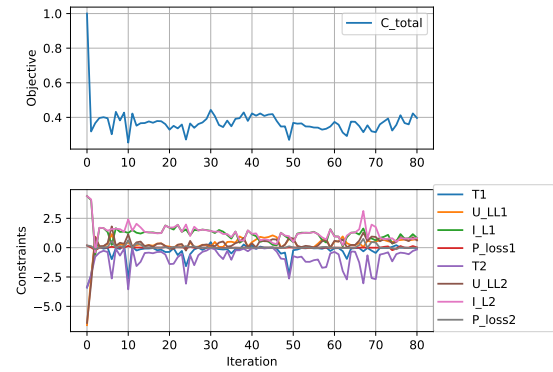
Figure 5.10: Optimization with Demagnetization Constraint



(a) The optimum design.

(b) The **partial** change in objective and constraints during optimization.**Figure 5.11:** Optimization for Demagnetized Machine

(a) The optimum design.

(b) The **partial** change in objective and constraints during optimization.**Figure 5.12:** Optimization for Demagnetized Machine and its Normal Operating Point

From these figures we can clearly see that the machine's geometry changes with the different optimization procedures. The magnet size is greatly influenced. From Table F.2 it can be seen that all torque outputs for the initial steady-state conditions is able to be around 200 Nm and a new operating point after a three-phase short-circuit is found. This means an optimum machine can be found that is capable of maintaining its performance

	Normal	Demagnetization Constraint	Demagnetized Machine	Normal Operating Point and Demagnetized
Total Cost (US\$)	114,73	118,29	145,83	139,49
Outer Radius of Stator (mm)	125	125	125	125
Stack Length (mm)	80	80	98,28	85,7

Table 5.3: Some parameters of the optimized machines.

after a three-phase short-circuit occurs.

The optimization takes a lot longer when taking a three-phase short-circuit into account. However, previously a transient FEM would be required to only determine the effect of a three-phase short-circuit. Now this three-phase short-circuit can even be practically taken into account during optimization, i.e. when applying it.

In Table 5.3 some of the output parameters is shown. In all the different optimization techniques an upper bound for the outer radius of 125 mm were reached. While normal optimization and optimization with a demagnetization constraint can fulfill all specifications while using the lower boundary of the stack length of 80 mm, the two new techniques require a longer stack length. Because the magnet size increases for optimization with a demagnetized or normal and demagnetized machine, the cost also increases.

Chapter 6

Conclusion

6.1. Summary

During this project, a PMSM was analysed after a three-phase short-circuit occurred. The dq-currents were accurately determined without a transient FEA, by solving differential equations with the Runge-Kutta fourth order method. From these transient dq-currents the worst-case operating point can be extracted and its effect on the demagnetization and performance of the PMSM can be determined. Furthermore, a PMSM can now be optimized w.r.t. this worst-case demagnetization. It can also be short-circuited multiple times.

The dq-currents' behaviour corresponded well with what was expected in prior research [3]. It did not entirely correspond with that of a transient FEA, however, there is significant similarities with multiple reasons for any differences.

An analytical method, making use of inductance maps, can also be used to determine dq-currents after a three-phase short-circuit. This methodology depends heavily on the density of the flux linkage maps.

6.2. Objectives

During this project the following objectives were achieved:

1. **DQ-Currents after Three-Phase Short Circuit** - In subsection 3.2, the methodology to obtain dq-currents after a three-phase short-circuit occur is explained. This is tested in chapter 4.
2. **Effect of Worst-Case Operating Point** - When implementing the analysis of demagnetization due to a three-phase short-circuit in section 5.1, it can be seen that

it corresponds well with a FEM used in the industry, Ansys Maxwell, although it is not exactly the same.

3. **Optimize w.r.t. Demagnetized PMSM** - In section 5.2 optimization whilst taking into account the effect of permanent demagnetization is explained and demonstrated.

6.3. Observations

- A three-phase short-circuit has a negative effect on a PMSM due to the demagnetization effect on the permanent magnet. During a three-phase short-circuit, the d-axis current becomes extremely negative, causing a MMF that damages this permanent magnet. After this short-circuit occurs, the PMSM is not able to function within its specifications. These three-phase short-circuits can occur often due to the external controlling electronics.
- Two different methods were used to determine the dq-currents after a three-phase short-circuit. The first method made use of solving differential equations with the Runge-Kutta 4th order method. This is the more dependable and accurate method. The second method made use of determining inductance maps at steady-state and use this to determine all required unknown variables in a characteristic mathematical equation that describes the dq-currents after a short-circuit occurs. This method is less accurate, due to being extremely dependable on a dense flux linkage map and depending on a lot of assumptions.
- This short circuit and the effect it has could previously only be determined by a Transient FEA. This FEA is extremely time-consuming and due to the nature of most FEM's, difficult to set up. To simulate a three-phase short-circuit in Ansys Maxwell, an external circuit or co-simulation with Simplorer is required. As soon as the external circuit is used, the PMSM is not controlled as in a normal simulation. Careful choices for frequencies, voltages, phase angles and current direction is required. It is not practical to simulate a three-phase short-circuit in this way when designing a PMSM, as the setup is tedious and constrained by the external circuit. During this project a method was implemented to determine the dq-currents after a short-circuit in SEMFEM. These dq-currents corresponded well with prior research [3] and also corresponded to some extent with an Ansys Maxwell Transient simulation. After these dq-currents were calculated, simulating its most negative d-axis current, together with the corresponding q-axis current in SEMFEM, allows an accurate determination of the demagnetizing effect it has on permanent magnet.
- It is now possible to simulate a three-phase short-circuit in SEMFEM. Because

it is now known what to expect after a three-phase short-circuit occurs, it is also possible to take this into account when optimizing a machine. The machine can be optimized to not only work during normal operation, but also remain within specifications after a three-phase short-circuit occurred. Previously, this was not possible as the effect of the three-phase short-circuit was unknown. A comparison between a previously designed machine and the new design which is able to operate within its specifications after a three-phase short-circuit occurs is shown in a Case Study in Appendix G. The new optimization influences the size of the magnet and the distance between the magnet and the coils. These PMSM's will now be more expensive to manufacture, however, replacement due to failure after a three-phase short-circuit will be less.

6.4. Implications

An analysis of a PMSM's demagnetization due to a three-phase short-circuit can be made in SEMFEM. This means a PMSM can be developed and designed, not only for its normal operating conditions, but also to behave optimally after a three-phase short-circuit.

6.5. Future Work

Possible future work can include the implementation of a phase-phase short-circuit, phase-to-earth short-circuit and phase-phase-to-earth short-circuit. The calculation of the inductances when calculating the analytical method can be refined. During optimization equal weight were given to the normal and demagnetized operation, i.e. operation before and after a three-phase short-circuit. It would be beneficial to optimize primarily for the normal operating point and have some specific calculation of the required specifications for use after a three-phase short-circuit occurs. The use of demagnetization due to a three-phase short-circuit in optimization has a lot of potential for future work.

Bibliography

- [1] C. Andrews, “Understanding permanent magnets,” 10 1995, pp. 311 – 315.
- [2] D. Egorov, “Analytic evaluation of three-phase short circuit demagnetization and hysteresis loss risk in rotor-surface- magnet permanent-magnet synchronous machines,” Ph.D. dissertation, 07 2015.
- [3] J. Germishuizen and C. Adam, “Integrating fem and existing traction motor design tools into an everyday engineering environment,” *e i Elektrotechnik und Informationstechnik*, vol. 136, 03 2019.
- [4] A. Eilenberger and M. SchrodL, “Sudden short-circuit analysis of a salient permanent magnet synchronous machine with buried magnets for traction applications,” 09 2010.
- [5] K. M. Inc., *Demagnetization (BH) Curves for Neodymium Magnets*, unknown (accessed August 7, 2020). [Online]. Available: <https://www.kjmagnetics.com/bhcurves.asp>
- [6] J. Hong, D. Hyun, S. B. Lee, J. Yoo, and K. Lee, “Automated monitoring of magnet quality for permanent-magnet synchronous motors at standstill,” *IEEE Transactions on Industry Applications*, vol. 46, no. 4, pp. 1397–1405, 2010.
- [7] J. Haylock, U. Hoefer, and A. Jack, “Predicting and preventing demagnetisation in permanent magnet motor drives,” 04 2006, pp. 474 – 478.
- [8] G. Choi and T. Jahns, “Demagnetization characteristics of permanent magnet synchronous machines,” *Proceedings, IECON 2014 - 40th Annual Conference of the IEEE Industrial Electronics Society*, pp. 469–475, 10 2014.
- [9] S. Gerber, personal communication.
- [10] P. Virtanen, R. Gommers, T. E. Oliphant, M. Haberland, T. Reddy, D. Cournapeau, E. Burovski, P. Peterson, W. Weckesser, J. Bright, S. J. van der Walt, M. Brett, J. Wilson, K. Jarrod Millman, N. Mayorov, A. R. J. Nelson, E. Jones, R. Kern, E. Larson, C. Carey, Í. Polat, Y. Feng, E. W. Moore, J. Vand erPlas, D. Laxalde, J. Perktold, R. Cimrman, I. Henriksen, E. A. Quintero, C. R. Harris, A. M. Archibald, A. H. Ribeiro, F. Pedregosa, P. van Mulbregt, and S. . . Contributors, “SciPy 1.0: Fundamental Algorithms for Scientific Computing in Python,” *Nature Methods*, vol. 17, pp. 261–272, 2020.

- [11] J. Germishuizen and R. Tanner, “Calculating the pm motor inductances using the two-dimensional flux linkages,” *International Journal of Applied Electromagnetics and Mechanics*, vol. 57, pp. 1–8, 03 2018.
- [12] M. K. Heris, “Runge-kutta method: Theory and python + matlab implementation,” <https://www.youtube.com/watch?v=1FYrnwqWQNY>, accessed: 2020-09-01.
- [13] A. Shahat and H. SHEWY, “Pm synchronous motor dynamic modeling,” 12 2009.
- [14] R.-J. W. Stavros Pastellides, Stiaan Gerber and M. J. Kamper, *Design of a Surface-Mounted PM Motor for Improved Flux Weakening Performance*, vol. 57, pp. 1–7.

Appendix A

Project Planning Schedule

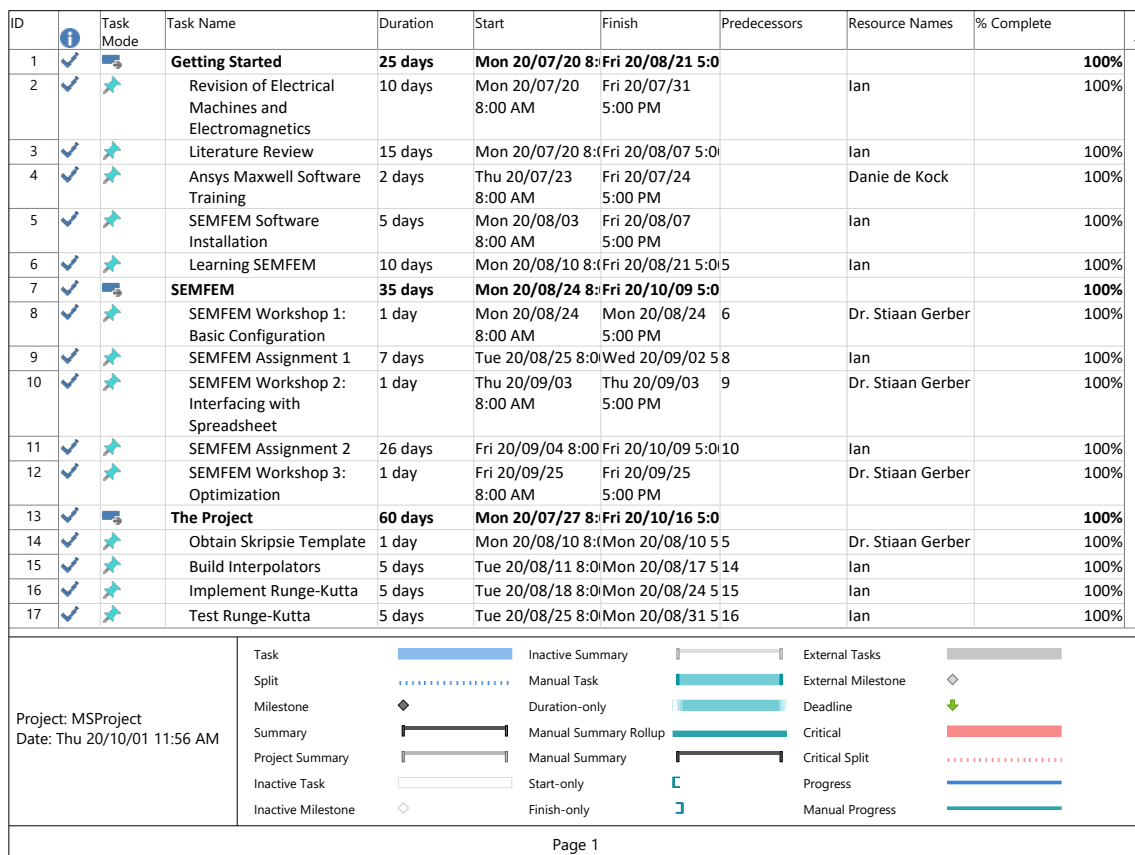


Figure A.1: Planning 1.a

ID	Task Mode	Task Name	Duration	Start	Finish	Predecessors	Resource Names	% Complete
18		Develop Root function	5 days	Tue 20/09/01 8:00	Mon 20/09/07 5:17	17	Ian	100%
19		Recreate Germishuizen's Machine from Scratch in SEMFEM	5 days	Tue 20/08/11 8:00 AM	Mon 20/08/17 5:00 PM	14	Ian	100%
20		Build an Ansys Maxwell Model for Verification	10 days	Mon 20/07/27 8:00 AM	Fri 20/08/07 5:00 PM	4	Ian	100%
21		Implement Demagnetization in SEMFEM	10 days	Mon 20/09/07 8:00 AM	Fri 20/09/18 5:00 PM	18	Ian	100%
22		Verify Results	10 days	Mon 20/09/21 8:00	Fri 20/10/02 5:00	20,21	Ian	100%
23		Case Study	10 days	Mon 20/10/05 8:00	Fri 20/10/16 5:00	22	Ian	100%
24		Reporting	80 days	Mon 20/07/20 8:00	Fri 20/11/06 5:00			100%
25		Do all Reporting extra's: ELO, Planning Schedule, Plagiarism, etc.	1 day	Mon 20/07/20 8:00 AM	Mon 20/07/20 5:00 PM		Ian	100%
26		Report Writing	80 days	Mon 20/07/20 8:00	Fri 20/11/06 5:00		Ian	100%
27		Hand-in's	6 days	Mon 20/11/09 8:00	Mon 20/11/16 5:00			0%
28		Project Hand-in	0 days	Mon 20/11/09 11:00	Mon 20/11/09 12:00			100%
29		Oral Presentations	5 days	Mon 20/11/09 8:00	Fri 20/11/13 5:00	28		0%
30		Slides with Presentation Upload	0 days	Mon 20/11/16 8:00 AM	Mon 20/11/16 8:00 AM	29		0%
31		Project Open Day	1 day	Mon 20/11/16 8:00	Mon 20/11/16 5:30			0%
<div> <div>Project: MSPProject Date: Thu 20/10/01 11:56 AM</div> <div> <div>Task</div> <div>Split</div> <div>Milestone</div> <div>Summary</div> <div>Project Summary</div> <div>Inactive Task</div> <div>Inactive Milestone</div> </div> <div> <div>Inactive Summary</div> <div>Manual Task</div> <div>Duration-only</div> <div>Manual Summary Rollup</div> <div>Manual Summary</div> <div>Start-only</div> <div>Finish-only</div> </div> <div> <div>External Tasks</div> <div>External Milestone</div> <div>Deadline</div> <div>Critical</div> <div>Critical Split</div> <div>Progress</div> <div>Manual Progress</div> </div> </div>								
Page 2								

Figure A.2: Planning 1.b

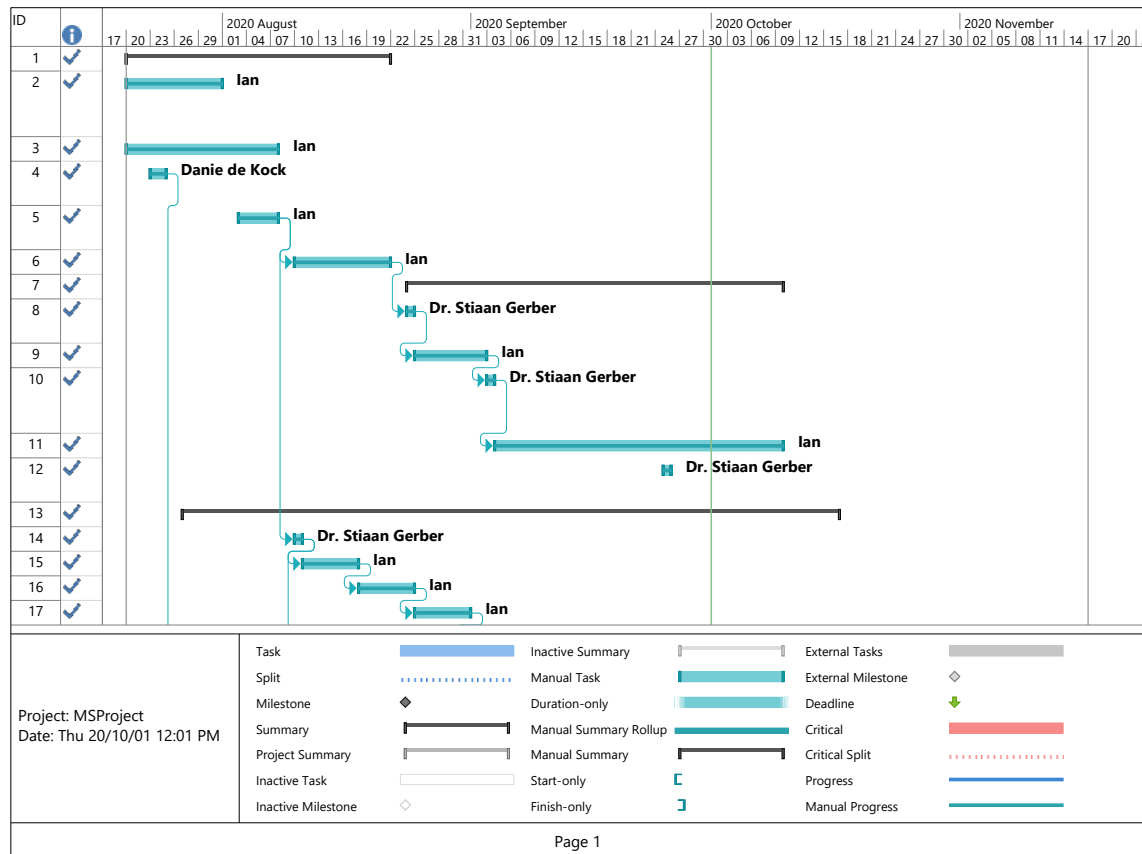


Figure A.3: Planning 2.a

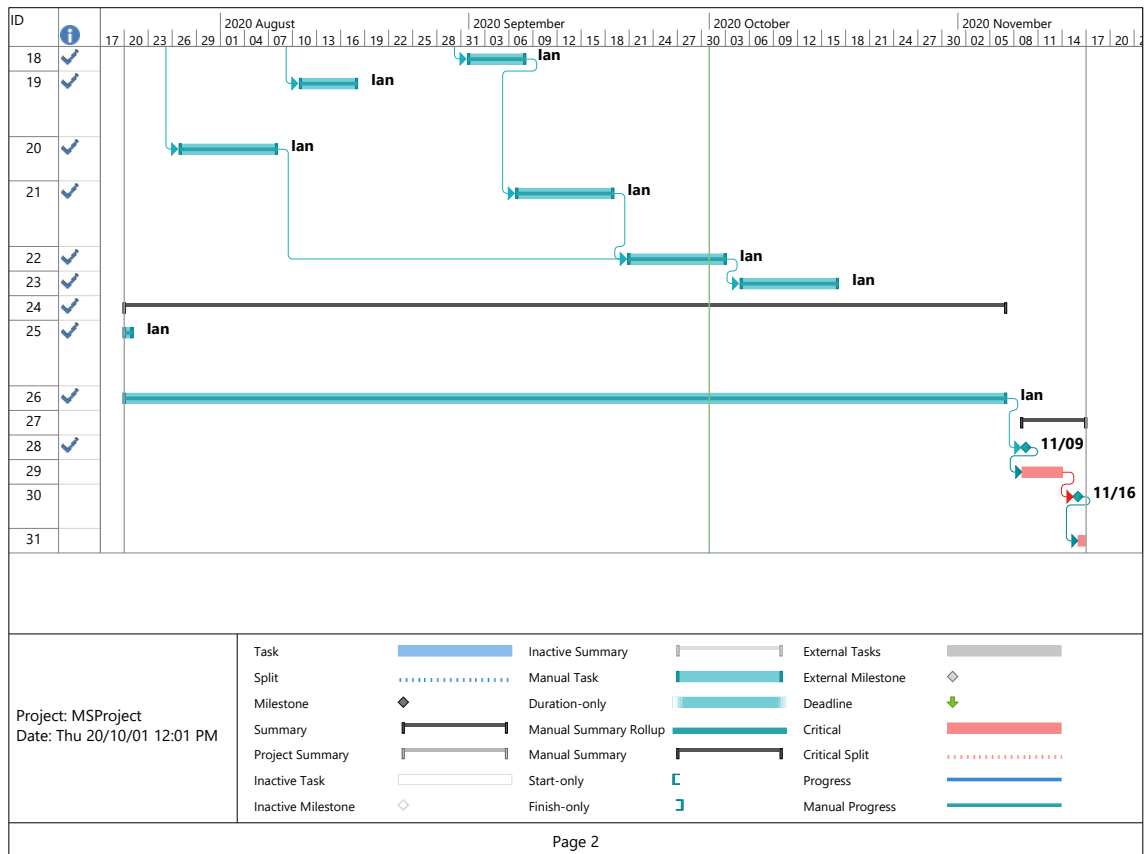


Figure A.4: Planning 2.b

Appendix B

Outcomes Compliance

B.1. Exit Level Outcome 1: Problem Solving

Electrical machines are a very specific field with a lot of different areas to investigate. As our knowledge in this field increase with a greater speed than ever before, multiple areas remain without in-depth research. In chapter 1 the author has thoroughly identified and explained the problem, which was only constructed on a high-level, with multiple additional hurdles and complexities as the project progressed. In this chapter, the author also explained the background and the proposed methodology. He has analyzed this problem in chapter 3 and gave the solutions to the complex problems that was formulated in chapter 1 in chapter 3. These solutions were not readily available. Some similar research was done, thus some guidelines were available from multiple sources, but the approach was unique. SEMFEM, in which these methodologies were implemented, did not have any solutions for dq-currents after a three-phase short-circuit, inductance calculations. The author was left to decide on his own design and implementation on these sections with the guide of his supervisors. The solutions required a large scope of knowledge w.r.t. PMSM's.

B.2. Exit Level Outcome 2: Application of scientific and engineering knowledge

In chapter 3 the space vector theory together with the magnetic circuit of a PMSM were used in various ways to implement solutions. The equations that describe these theories were then used to provide numerical, analytical and computational solutions in chapter 3. This was done in Python.

B.3. Exit Level Outcome 3: Engineering design

In chapter 3 the methodology and system are described to solve the identified problem. The author made use of a methodology to provide an accurate demagnetization analysis. This was done with the aid of previously identified procedures and some innovative practices, as described in chapter 3. The system was synthesized by integrating various detailed components.

B.4. Exit Level Outcome 4: Investigations, experiments and data analysis

In chapter 4 multiple methods were used outside the scope of the project to verify certain units of the approach. The Runge-Kutta method was tested on entirely different differential equations in section 4.1. The dynamic behaviour was tested by recreating a complex machine from scratch with minimal information in section 4.1. The analytical approach was then compared to this outcome in section 4.3. Finally, a detailed verification was made in chapter 5 to verify results.

B.5. Exit Level Outcome 5: Engineering methods, skills and tools, including information technology

Various additional engineering methods were applied during this project. The author had to install a new operating system (OS), Linux, to be able to run SEMFEM on his laptop. He had to install Python and change multiple settings to make SEMFEM compatible with this interface. He had to become acquainted with the SEMFEM interface as well as obtain in depth knowledge of its libraries, as his project had to use some of SEMFEM's built-in functions.

The author also had to learn to use a complex FEM tool, Ansys Maxwell, to verify his results. He had to install this on his laptop using a VPN (Virtual Private Network) and when Ansys Maxwell did not work anymore due to licensing issues, he had to make use of TeamViewer to access it. The author also made use of a Latex editor and Microsoft Teams.

B.6. Exit Level Outcome 6: Professional and technical communication

The author engaged in weekly meetings with his supervisors via Microsoft Teams, demonstrating sufficient communication to obtain enough information to complete this project. This document serves as the professional reporting required, while the oral and open day is yet to be conducted.

B.7. Exit Level Outcome 8: Individual work

During the course of this project, the author worked mainly from home. The only interaction with supervisors were weekly meetings between 30 minutes and an hour. No physical meetings were conducted. The author managed to gain all required information on his own, perform all the required analysis and solutions and overcome all problems during this time, with the help of his supervisors.

B.8. Exit Level Outcome 9: Independent learning ability

The author has shown that he could use the knowledge he has obtained at Stellenbosch University since 2017 to apply on a practical problem. With limited knowledge of machines, with only Energy System 344 being applicable to this field of study from all the modules studied up until now, the author managed to complete this project. He was able to do this with solutions in a relatively unknown field of research with the required knowledge of the implications of this work in the traction motor industry.

Appendix C

Machines Used

The following table describes some of the machines used during this project.

Parameter	Machine 1	Machine 2	Machine 3	Machine 4 (initial)
Poles	12	4	4	4
Slots	54	48	24	48
Stack length (m)	0.4	0.089	0.2	0.091
Magnetic Pole Pitch (d)	0.95	0.95	0.8	0.79
Coil Span	5	5	5	5
Number of Coil Layers	2	2	1	2
Fill Factor (d)	0.97	0.65	0.75	0.65
Rotor Inner Radius (m)	0.265	0.0659	0.0.013	0.029
Rotor Outer Radius (m)	0.322	0.9048	0.037	0.107
Air Gap Length (m)	0.001	0.001	0.0005	0.0001
Stator Outer Radius (m)	0.2	0.125	0.06	0.125
Remanent Flux Density (T)	1.115	1.184	1.18	1.18
Coil Turns	2	5	52	5.34
Stator Slot Type	Straight	Straight	Round	Straight
Rotor Slot Tooth Type	Straight	V-shaped	Outer	V- shaped
ω (rad/s)	830	5000	1000	4000

Table C.1: The specifications of the different machines used in this project.

Appendix D

Information for Runge-Kutta 4'th Order Unit Verification

In the article [13], typical values for a Kollmorgen 6-pole PM synchronous motor driven into saturation is given:

$$I_s = 10 \text{ to } 20 \text{ A}$$

$$\theta_m = 0^\circ \text{ to } 90^\circ$$

$$R_s = 0.95 \, \Omega$$

$$L_{qo} = 14.10 \text{ mH}, L_{do} = 8.13 \text{ mH}, \psi_{mo} = 0.277 \text{ Wb}$$

With ψ_m , the flux of the permanent magnet and where the derivative of the currents is a function of the inductances, while the inductances are also dependent on the currents:

$$L_d = 8.13 \frac{63.3 + 10}{63.3 + i_q}$$

$$L_q = 14.10 \frac{21.3 + 10}{21.3 + i_q}$$

$$\psi_m = 0.277 \frac{63.3 + 10}{63.3 + i_q}$$

Appendix E

Reference Guide

All of the following functions are implemented in the class: skripsie. The class is in the file: skripsie_file.py, which should be in the same directory as the executing .py file and should be imported as:

```
1 import skripsie_file.skripsie
```

E.1. Interpolators

E.1.1. Obtaining Interpolators

Although SEMFEM already has interpolation functions implemented, this function is specifically built, aimed at demagnetization computations and are suggested to use.

```
1 class skripsie.interp(i_d, i_q, fl_d, fl_q)
```

More can be read in subsection 3.2.1.

Parameters:

- `i_d` : array of d-axis currents in Ampere, array(N,).
- `i_q` : array of q-axis currents in Ampere, array(N,).
- `fl_d` : array of d-axis flux linkages in Wb-t, array(N,).
- `fl_q` : array of q-axis flux linkages in Wb-t, array(N,).

Returns:

- `I.D` : grid of d-axis currents in Ampere, array(N, N).
- `I.Q` : grid of q-axis currents in Ampere, array(N, N).

- FL_D : Output for d-axis flux linkage interpolator in Wb-t, object: LinearNDInterpolator.
- FL_Q : Output for q-axis flux linkage interpolator in Wb-t, object: LinearNDInterpolator.
- FL_D_DRAW : grid of d-axis flux linkage in Wb-t specifically for drawing the interpolator, array(N, N).
- FL_Q_DRAW : grid of q-axis flux linkage in Wb-t specifically for drawing the interpolator, array(N, N).

E.2. Runge-Kutta

The following functions concern the calculation of the dq-currents by means of integration.

E.2.1. Obtaining Dynamic Behaviour for Specified Time Period

This function calculates the behaviour of dq-currents after a three-phase short-circuit occurred. This is done up to a specified final time. When investigating demagnetization, interest are specifically in the minimum d-axis current. This minimum can be expected to be obtained within the first period, and a suitable final time would be $\frac{120}{n_{sp}}$. It is important to first run the interp-function described in subsection E.1.1 to obtain the required input parameters.

```
1 def crux(dt, R_s, omega, FL_D, FL_Q, i_d_in, i_q_in, tf, t0 = 0,
    plotter = True)
```

More can be read in subsection 3.2.2.

Parameters:

- dt : Time step in seconds, float.
- R_s : Synchronous Resistance in Ω , float.
- omega : Electrical radial frequency, integer.
- FL_D : Output for d-axis flux linkage interpolator in Wb-t, object: LinearNDInterpolator.
- FL_Q : Output for q-axis flux linkage interpolator in Wb-t, object: LinearNDInterpolator.
- i_d_in : Starting d-axis current operating point in Ampere, float.

- `i_q_in` : Starting q-axis current operating point in Ampere, float.
- `tf` : Final Time in seconds, float. A value of $\omega/60$ is proposed.
- `t0` : Starting time in seconds, set at 0 seconds, float.
- `plotter` : Boolean, True if dynamic behaviour should be printed.

Returns:

- `i_d` : transient d-axis current behaviour after short circuit in Ampere, `array(n,)`.
- `i_q` : transient q-axis current behaviour after short circuit in Ampere, `array(n,)`.
- `t` : time vector containing corresponding time in seconds for dq-currents, `array(n,)`.
- `minimum_d` : Most negative d-axis current in Ampere, float.
- `minimum_q` : Q-axis current in Ampere, corresponding to most negative d-axis current, float.

E.2.2. Obtaining Dynamic Behaviour until First Minimum

This function only calculates the dq-currents until the first minimum is reached. This function is quicker, but may be less accurate over a wide variety of machine characteristics.

```
1 def crux_eff_change(dt, R_s, omega, FL_D, FL_Q, i_d_0, i_q_0, t0 = 0,
    plotter = True)
```

More can be read in section 3.8.

Parameters:

- `dt` : Time step in seconds, float.
- `R_s` : Synchronous Resistance in Ω , float.
- `omega` : Electrical radial frequency, integer.
- `FL_D` : Output for d-axis flux linkage interpolator in Wb-t, object: `LinearNDInterpolator`.
- `FL_Q` : Output for q-axis flux linkage interpolator in Wb-t, object: `LinearNDInterpolator`.
- `i_d_in` : Starting d-axis current operating point in Ampere, float.
- `i_q_in` : Starting q-axis current operating point in Ampere, float.
- `tf` : Final Time in seconds, float. A value of $\omega/60$ is proposed.

- `t0` : Starting time in seconds, set at 0 seconds, float.
- `plotter` : Boolean, True if dynamic behaviour should be printed.

Returns:

- `i_d` : transient d-axis current behaviour after short circuit in Ampere, array(n,).
- `i_q` : transient q-axis current behaviour after short circuit in Ampere, array(n,).
- `t` : time vector containing corresponding time in seconds for dq-currents, array(n,).
- `minimum_d` : Most negative d-axis current in Ampere, float.
- `minimum_q` : Q-axis current in Ampere, corresponding to most negative d-axis current, float.

E.3. Analytical Approach

E.3.1. Obtaining Dynamic Behaviour

The following function combines all the functions required to obtain the dynamic short circuit currents with the analytical approach. It is very important to have a extremely fine flux linkage map when using this approach. This is due to the inductance maps required. These inductances can change rapidly, necessitating the use of this densely populated maps. Due to the calculation of the steady state inductances, the function be time consuming. Furthermore, it is not extremely accurate.

```
1 skripsie.get_analytical(i_d, i_q, FL_D, FL_Q, i_d_start, i_q_start, R_s,
    phase_A_offset, alpha, omega, t, plotter = False)
```

More can be read in section 3.4. **Parameters:**

- `i_d` : array of d-axis currents in Ampere, array(N,).
- `i_q` : array of q-axis currents in Ampere, array(N,).
- `FL_D` : Output for d-axis flux linkage interpolator in Wb-t, object: LinearNDInterpolator.
- `FL_Q` : Output for q-axis flux linkage interpolator in Wb-t, object: LinearNDInterpolator.
- `i_d_start` : Starting d-axis current operating point in Ampere, float.

- `i_q_start` : Starting q-axis current operating point in Ampere, float.
- `R_s` : Synchronous Resistance in Ω , float.
- `phase_A_offset` : Phase offset angle in radians, float.
- `alpha` : angle between reference stator axis and permanent magnet's flux linkage vector.
- `omega` : Electrical radial frequency, integer.
- `t` : time vector containing corresponding time in seconds for dq-currents, `array(n,)`.
- `plotter` : Boolean, True if dynamic behaviour should be printed.

Returns:

- `i_d` : transient d-axis current behaviour after short circuit in Ampere, `array(n,)`.
- `i_q` : transient q-axis current behaviour after short circuit in Ampere, `array(n,)`.
- `t` : time vector containing corresponding time in seconds for dq-currents, `array(n,)`.
- `minimum_d` : Most negative d-axis current in Ampere, float.
- `minimum_q` : Q-axis current in Ampere, corresponding to most negative d-axis current, float.

Appendix F

Optimizing Results

Table F.1 contains the initial configuration, bounds and type of input/output to the optimization. Table F.2 contains the resulting outputs with:

1. Optimize 1 - Normal Optimization.
2. Optimize 2 - Optimization with Demagnetization Constraint.
3. Optimize 3 - Optimization for Demagnetized Machine.
4. Optimize 4 - Optimization for Demagnetized Machine and its Normal Operating Point.

Input	Low Worst	Low Bound	Initial	Up Bound	Up Worst	Type
mpp		200,00E-03	312,94E-03	950,00E-03		Variable
ro_split		300,00E-03	709,16E-03	900,00E-03		Variable
st_tt_split		300,00E-03	475,06E-03	900,00E-03		Variable
mbt			1,00E-03			Constant
sbt		2,00E-03	4,64E-03	7,00E-03		Variable
obt			1,00E-03			Constant
mtheta_pp		50,00E-03	975,37E-03	980,00E-03		Variable
p6pp		50,00E-03	478,24E-03	900,00E-03		Variable
sgt			500,00E-06			Constant
sop		200,00E-03	520,73E-03	800,00E-03		Variable
sat			1,00E-03			Constant
sot			1,00E-03			Constant
R			125,00E-03			Constant
r_min		20,00E-03	34,69E-03	50,00E-03		Variable
L		80,00E-03	129,91E-03	130,00E-03		Variable
agl			1,00E-03			Constant
p			4,00E+00			Constant
Q			48,00E+00			Constant
N_L			2,00E+00			Constant
N_S			5,00E+00			Constant
Br			1,18E+00			Constant
mur			1,05E+00			Constant
coil_ff			650,00E-03			Constant
coil_turns		1,00E+00	1,41E+00	10,00E+00		Variable
mesh_scale			3,00E+00			Constant
gap_layers			1,00E+00			Constant
steps			8,00E+00			Constant

verbosity			0,00E+00			Constant
nrpm0			4,00E+03			Constant
nrpm1			5,00E+03			Constant
nrpm2			5,00E+03			Constant
idens_d1	-30,00E+00		-18,81E+00	-1,00E+00		Variable
idens_q1	1,00E+00		14,18E+00	30,00E+00		Variable
idens_d2	-30,00E+00		-17,92E+00	-1,00E+00		Variable
idens_q2	1,00E+00		13,47E+00	30,00E+00		Variable
winding_temp			150,00E+00			Constant
wge			1,00E-03			Constant
wd			5,00E-03			Constant
Output Variables						
C_total			212,31E+00			Objective
C_steel			61,89E+00			Output
C_copper			33,34E+00			Output
C_magnet			117,09E+00			Output
M_total			38,28E+00			Output
M_steel			30,94E+00			Output
M_copper			5,00E+00			Output
M_magnet			2,34E+00			Output
LL			177,14E-03			Output
T1	150,00E+00	200,00E+00	197,91E+00			Constraint
T_rip1			677,15E-03			Output
P1			104,80E+03			Output
U_LL1			233,40E+00	230,00E+00	300,00E+00	Constraint
LL1			312,47E+00	500,00E+00	600,00E+00	Constraint
L_dens1			16,66E+00			Output
L_theta_deg1			143,49E+00			Output
P_copper1			4,04E+03			Output
P_core1			702,07E+00			Output
P_loss1			4,74E+03	4,20E+03	8,00E+03	Constraint
eff1			956,75E-03			Output
PF1			869,42E-03			Output
demag_margin1			352,59E-03			Output
f_e1			333,33E+00			Output
T2	150,00E+00	200,00E+00	141,26E+00			Constraint
T_rip2			654,39E-03			Output
P2			71,17E+03			Output
U_LL2			244,53E+00	230,00E+00	300,00E+00	Constraint
LL2			296,13E+00	500,00E+00	600,00E+00	Constraint
L_dens2			15,85E+00			Output
L_theta_deg2			143,88E+00			Output
P_copper2			3,65E+03			Output
P_core2			727,91E+00			Output
P_loss2			4,38E+03	4,20E+03	8,00E+03	Constraint
eff2			942,01E-03			Output
PF2			636,55E-03			Output
demag_margin2			483,18E-03			Output
f_e2			333,33E+00			Output
ewf			716,30E-03			Output

Table F.1: Optimize Spreadsheet Inputs and Outputs Configuration. The only difference would be for optimizing with a demagnetization constraint where a constraint would be added.

Input	Optimized 1	Optimized 2	Optimized 3	Optimized 4
project	project	project	project	project
mpp	950,00E-03	851,01E-03	484,88E-03	581,59E-03
ro_split	626,77E-03	619,31E-03	617,05E-03	567,68E-03
st_tt_split	493,14E-03	470,46E-03	548,57E-03	504,02E-03
mbt	1,00E-03	1,00E-03	1,00E-03	1,00E-03
sbt	6,64E-03	6,79E-03	4,65E-03	6,35E-03
obt	1,00E-03	1,00E-03	1,00E-03	1,00E-03
mtheta_pp	481,56E-03	544,59E-03	613,41E-03	853,78E-03
p6pp	185,52E-03	228,08E-03	317,56E-03	320,76E-03
sgt	500,00E-06	500,00E-06	500,00E-06	500,00E-06
sop	440,42E-03	430,36E-03	562,50E-03	476,46E-03
sat	1,00E-03	1,00E-03	1,00E-03	1,00E-03
sot	1,00E-03	1,00E-03	1,00E-03	1,00E-03
R	125,00E-03	125,00E-03	125,00E-03	125,00E-03
r_min	33,49E-03	34,09E-03	35,80E-03	41,98E-03
L	80,00E-03	80,00E-03	98,28E-03	85,70E-03
agl	1,00E-03	1,00E-03	1,00E-03	1,00E-03
p	4,00E+00	4,00E+00	4,00E+00	4,00E+00
Q	48,00E+00	48,00E+00	48,00E+00	48,00E+00
N_L	2,00E+00	2,00E+00	2,00E+00	2,00E+00
N_S	5,00E+00	5,00E+00	5,00E+00	5,00E+00
Br	1,18E+00	1,18E+00	1,18E+00	1,18E+00
mur	1,05E+00	1,05E+00	1,05E+00	1,05E+00
coil_ff	650,00E-03	650,00E-03	650,00E-03	650,00E-03
coil_turns	1,37E+00	1,35E+00	1,39E+00	1,17E+00
mesh_scale	3,00E+00	3,00E+00	3,00E+00	3,00E+00
gap_layers	1,00E+00	1,00E+00	1,00E+00	1,00E+00
steps	8,00E+00	8,00E+00	8,00E+00	8,00E+00
verbosity	0,00E+00	0,00E+00	0,00E+00	0,00E+00
nrpm0	4,00E+03	4,00E+03	4,00E+03	4,00E+03
nrpm1	5,00E+03	5,00E+03	5,00E+03	5,00E+03
nrpm2	5,00E+03	5,00E+03	-13,66E+00	5,00E+03
idens_d1	-15,48E+00	-15,33E+00	12,64E+00	-15,82E+00
idens_q1	17,37E+00	18,69E+00		15,18E+00
idens_d2				-14,63E+00
idens_q2				15,98E+00
winding_temp	150,00E+00	150,00E+00	150,00E+00	150,00E+00
wge	1,00E-03	1,00E-03	1,00E-03	1,00E-03
wd	5,00E-03	5,00E-03	5,00E-03	5,00E-03
Output				
C_total	114,73E+00	118,29E+00	145,83E+00	139,49E+00
C_steel	47,26E+00	46,85E+00	51,85E+00	44,25E+00
C_copper	27,16E+00	25,39E+00	43,12E+00	31,96E+00
C_magnet	40,32E+00	46,05E+00	50,86E+00	63,27E+00
M_total	28,51E+00	28,15E+00	33,41E+00	28,18E+00
M_steel	23,63E+00	23,42E+00	25,92E+00	22,13E+00
M_copper	4,07E+00	3,81E+00	6,46E+00	4,79E+00
M_magnet	806,33E-03	920,99E-03	1,02E+00	1,27E+00
LL	130,14E-03	129,42E-03	150,46E-03	136,75E-03
T1	199,74E+00	199,94E+00	199,87E+00	204,50E+00
T_rip1	219,99E-03	47,79E-03	190,24E-03	293,71E-03
P1	93,08E+03	97,12E+03	97,46E+03	103,05E+03
U_LL1	229,91E+00	230,05E+00	230,00E+00	182,98E+00
I_L1	336,33E+00	331,81E+00	373,44E+00	421,02E+00
I_dens1	16,45E+00	17,09E+00	13,16E+00	15,50E+00
I_theta_deg1	132,46E+00	130,09E+00	137,99E+00	136,80E+00

P_copper1	3,21E+03	3,23E+03	3,26E+03	3,35E+03
P_core1	989,02E+00	965,77E+00	949,51E+00	857,68E+00
P_loss1	4,20E+03	4,20E+03	4,21E+03	4,21E+03
eff1	956,87E-03	958,55E-03	958,64E-03	960,78E-03
PF1	827,44E-03	838,66E-03	744,79E-03	847,26E-03
demag_margin1	-282,58E-03	8,58E-03	250,97E-03	211,07E-03
f_e1	333,33E+00	333,33E+00	333,33E+00	333,33E+00
T2				199,91E+00
T_rip2				294,88E-03
P2				100,86E+03
U_LL2				191,69E+00
LL2				416,08E+00
L_dens2				15,32E+00
L_theta_deg2				133,20E+00
P_copper2				3,27E+03
P_core2				933,13E+00
P_loss2				4,20E+03
eff2				959,98E-03
PF2				802,03E-03
demag_margin2				266,31E-03
f_e2				333,33E+00
ewf	1,16E+00	1,15E+00	962,55E-03	1,08E+00

Table F.2: The Optimized Outputs.

Appendix G

Case Study

A traction motor for a Light Electric Vehicle (LEV) has been developed by a group of engineers at Stellenbosch University [14]. This machine was used as a case study to test the demagnetization analysis. First it was three-phase short-circuited multiple times to see how the performance is affected. Tables G.1 and G.2 shows the change in output torque and efficiency after multiple short-circuits at the normal operating speed, as well as the maximum operating speed. This is a practical way to look at the performance of the machine after a short-circuit. After a short-circuit occurs the machine is re-used with the same inputs. As seen in these tables the performance is greatly influenced. The most devastating influence is due to the first three-phase short-circuit. After the first short-circuit occurs, the torque performance stays relative constant. It is also evident that the PMSM is not operating efficient anymore after a short-circuit.

	Steady-State	After 1'st Short-Circuit	After 2'nd Short-Circuit	After 3'rd Short-Circuit	After 4'th Short-Circuit	After 5'th Short-Circuit
Torque (Nm)	19.540	8.968	8.971	8.968	8.958	8.941
Efficiency	0.911	0.825	0.821	0.818	0.814	0.811

Table G.1: The torque and efficiency output after multiple short-circuits at the normal operating speed.

	Steady-State	After 1'st Short-Circuit	After 2'nd Short-Circuit	After 3'rd Short-Circuit	After 4'th Short-Circuit	After 5'th Short-Circuit
Torque (Nm)	5.833	1.764	1.545	1.322	1.095	0.865
Efficiency	0.911	0.732	0.703	0.668	0.623	0.565

Table G.2: The torque and efficiency output after multiple short-circuits at full speed.

This PMSM can also be optimized for its normal operating point and for operation after a short-circuit. The different configurations can be see in Fig. G.1. It is evident that a bigger magnet works better and that the winding slots need to be spaced further. As seen in Tables G.3 and G.4 the performance after a short-circuit can now still be within specifications.



(a) The machine configuration after optimizing for a normal operating point.

(b) The machine configuration after optimizing for a demagnetized machine and the normal operating point.

Figure G.1: The machine configuration after optimizing for different operating points w.r.t. demagnetization.

	Steady-State	After 1'st Short-Circuit	After 2'nd Short-Circuit	After 3'rd Short-Circuit	After 4'th Short-Circuit	After 5'th Short-Circuit
Torque (Nm)	19.545	20.063	20.584	21.073	21.527	21.948
Efficiency	0.911	0.908	0.905	0.902	0.898	0.895

Table G.3: The torque and efficiency output after multiple short-circuits at normal speed for the new machine.

	Steady-State	After 1'st Short-Circuit	After 2'nd Short-Circuit	After 3'rd Short-Circuit	After 4'th Short-Circuit	After 5'th Short-Circuit
Torque (Nm)	5.827	6.400	6.873	7.197	7.205	6.976
Efficiency	0.909	0.910	0.908	0.904	0.897	0.886

Table G.4: The torque and efficiency output after multiple short-circuits at full speed for the new machine.